Journal of Medicinal Chemistry

Article

Highly Potent Non-Carboxylic Acid Autotaxin Inhibitors Reduce Melanoma Metastasis and Chemotherapeutic Resistance of Breast Cancer Stem Cells

Souvik Banerjee, Derek D. Norman, Sue Chin Lee, Abby L Parrill, Truc Chi T. Pham, Daniel L. Baker, Gabor G. Tigyi, and Duane D Miller

J. Med. Chem., **Just Accepted Manuscript** • DOI: 10.1021/acs.jmedchem.6b01270 • Publication Date (Web): 23 Jan 2017

Highly Potent Non-Carboxylic Acid Autotaxin Inhibitors Reduce Melanoma Metastasis and Chemotherapeutic Resistance of Breast Cancer Stem Cells

Souvik Banerjee,[1] Derek D. Norman,[2] Sue Chin Lee,[2] Abby L. Parrill,[3,4] Truc Chi T. Pham[3], Daniel L. Baker,[3] Gabor G. Tigyi[#,2] Duane D. Miller[*#.1]

1. Department of Pharmaceutical Sciences, College of Pharmacy, University of Tennessee Health Science Center, Memphis, TN 38163, USA
2. Department of Physiology, College of Medicine, University of Tennessee Health Science Center, Memphis, TN 38163, USA
3. Department of Chemistry, The University of Memphis, Memphis TN 38152
4. Computational Research on Materials Institute, The University of Memphis, Memphis TN 38152

[#] Senior co-authors

Address correspondence to: Duane D. Miller, Ph.D.
Email. dmiller@uthsc.edu
Phone. (+1)-901-448-6026Fax. (+1)-901-448-3446
or
Gabor Tigyi :Ph.D., M.D.
Email. gtigyi@uthsc.edu
Phone. (+1)-901-448-2634

ABSTRACT

Autotaxin (ATX, aka. ENPP2) is the main source of the lipid mediator lysophosphatidic acid (LPA) in biological fluids. This study reports on inhibitors of ATX derived by lead optimization of the benzene-sulfonamide *in silico* hit compound **3**. The new analogues provide a comprehensive SAR of the benzene-sulfonamide scaffold that yielded a series of highly potent ATX inhibitors. The three most potent analogues (**3a,** IC_{50} ~ 32 nM and **3b,** IC_{50} ~ 9 nM as well as **14,** IC_{50} ~ 35 nM) inhibit ATX-dependent invasion of A2058 human melanoma cells *in vitro*. Two of the most potent compounds, **3b** and **3f** (IC_{50} ~ 84 nM) lack inhibitory action on ENPP6 and ENPP7 but possess weak antagonist action specific to the LPA_1 GPCR. In particular, compound **3b** potently reduced *in vitro* chemotherapeutic resistance of 4T1 breast cancer stem-like cells to paclitaxel and reduced significantly B16 melanoma metastasis *in vivo*.

Key words: ATX, LPA, chemoresistance, cancer stem cell, metastasis, benzene sulfonamide

Introduction.

Autotaxin (ATX), a member of the ectonucleotide pyrophosphate and phosphatase (ENPP) family, is primarily known to catalyze the hydrolysis of lysophosphatidylcholine (LPC) resulting in the production of the growth-factor-like bioactive phospholipid lysophosphatidic acid (LPA).[1-3] LPA activates a set of six GPCR LPA_{1-6}, ion channels, the transcription factor PPARγ, which regulate a host of cellular responses, including cell proliferation and migration, vascular tone, and platelet aggregation.[4, 5] Many of these responses are at the core of human diseases that include fibrotic diseases, neuropathic pain, rheumatoid arthritis, as well as cardiovascular diseases.[1, 4-6] In recent years, the ATX-LPA signaling pathway has been linked to several aspects of cancer cell biology that include cancer growth, invasion, metastasis, and therapeutic resistance.[6-8] Recently, ATX has been found to play an important role in the maintenance and proliferation of ovarian cancer stem cells.[9] Because of the explicit role of LPA in these human pathologies development of drug-like ATX inhibitors has begun.[1, 3, 10-15]These synthetic efforts have resulted in a number of novel ATX inhibitors that can arbitrarily be divided into two categories: Lipid-like ATX inhibitors, that mimic either the LPC or LPA and; Non-lipid ATX inhibitors[1-3, 7, 11, 12, 14, 16-20]. Despite these efforts, limited success has been achieved in preclinical and regulatory development of ATX inhibitor drug candidates.[1] In this context, the high partition coefficient (Log P > 5) renders most lipid-like inhibitors unsuitable for potential clinical development.[2, 7, 16] The elucidation of ATX crystal structure with the inhibitor co-crystalized in the active site, provided insight into the potential active site surfaces.[10] We and others pursued rational discovery that yielded a new generation of small molecule drug-like non-lipid ATX inhibitors with

pharmacological properties that meet Lippinski's rule of five.[1, 6, 16, 18] A subgroup of recently developed non-lipid ATX inhibitors, including (*Z*)-4-[(4-{[3-(4-Fluorobenzyl)-2,4-dioxo-1,3-thiazolan-5-yliden]methyl}phenoxy) methyl]phenyl boronic acid (**HA 155)**[10], 3,5-Dichlorobenzyl-[4-[3-oxo-3-(2-oxo-2,3-dihydrobenzoxazol-6-yl)propyl]]piperazine-1-carboxylate (**PF 8380**)[23], compounds reported by pharmaceutical companies Novartis and PharmAkea , have similar structural features and contain an acid or acid-like moiety, to interact with one of the Zn^{2+} ions at the catalytic site, a core spacer, and a hydrophobic tail accommodated within the hydrophobic pocket of ATX.[1-3, 12, 21-24] However, to the best of our knowledge, none of the active site inhibitors have successfully made it through clinical trials yet. Thus, recent approaches have focused on developing small molecule non-lipid ATX inhibitors without an acidic moiety (Figure 1), allosteric modulators of the enzyme[15], and DNA aptamers.[25] Our group utilized high-throughput and in *silico* searching to identify a small molecule ATX inhibitor, 2,4-dichloro-*N*-(3-fluorophenyl)-5-(morpholinosulfonyl)benzamide [**GRI918013 (3), Figure 1A**], which exerts its inhibition by binding to the hydrophobic pocket remote from the catalytic site, and lacks an acidic moiety.[2, 16] This chemical entity, even without an acidic head group, shows the same pharmacological and biological effects as catalytic site inhibitors do but inhibition is mediated via interference with the binding of the hydrophobic chain of the lipid substrates, although it lacks sufficient potency and stability *in vivo*.[2, 16] Recently, Galapagos Inc., has developed a number of potent compounds that have a major structural similarity to **3**, lacking the acidic group (**Figure 1**).[3] One of the Galapagos compounds has been reported to successfully pass the first in-human phase one clinical trial. Thus, the objectives of our synthetic campaign were:

1) To improve the potency of ATX inhibition with IC_{50} values in the low nanomolar range and 2) Obtain compounds that were effective *in vitro* and *in vivo* assays dependent on ATX activity. Our lead optimization set four structural criteria for the novel compounds: 1) Lack of acidic moiety, 2) Lack of chiral center, 3) Molecular weight less than 500 D, and 4) Partition coefficients (Log P) less than 3. Here we report on the structure-activity relationship of several modifications of the hit **3** that yielded two novel compounds with potent *in vitro* and *in vivo* activity blocking B16 melanoma invasion, metastasis, and reduced chemotherapeutic resistance of 4T1 breast cancer stem-like cells to paclitaxel.

Results

1. Chemical synthesis

1.1. Modification of ring A. We designated the three rings in **3** as rings **A**, **B**, and **C** (**Figure 1A)**. Our previous screening experiments, mutagenesis, and molecular modelling findings suggested that **3** binds into the hydrophobic pocket of ATX without protruding into and blocking substrate access to the catalytic site as shown in **Figure 1B**. First, we designed and synthesized a series of derivatives with varying substituents on ring **A** as shown in **Scheme 1**.

Compound **3** was synthesized following the strategy described in **Scheme 1** with 70% yield. We first increased the number of fluorine substituents on ring A by synthesizing the 3,4-di-fluoro analogue (**3a)**, and the 3,4,5-tri-fluoro analogue (**3b)** depicted in **Scheme 1** and tested them for ATX inhibitory activity (**Table 1**). The simple manipulation of aromatic substituents resulted in four-fold IC_{50} improvements in **3a** (IC_{50} = 31 nM) and thirteen-fold in **3b** (IC_{50} = 9 nM) relative to the IC_{50}= 120 nM parent

compound. When **3b** was docked in to the ATX crystal structure (PDB **3NKM**)[22], we found that three fluoro substituents promote a tighter binding of this compound over **3** (**Figure 2)**. Top poses of these two compounds show strong volume overlap except in the angle of the halogenated ring A. **3** makes largely edge-to-face π interaction with residue W260 whereas, **3b** has a rotated aromatic ring that allows a hydrogen bond between a fluorine substituent and aromatic N-H of W260 (**Figure 3 A**). We continued this series by making penta-fluoro analogue (**3c**) that was poorly active. Next we synthesized and tested a relatively less electron deficient 3,4,5-trichloro analogue **3d**, and the electron donating 3,4,5-trimethoxy analogue **3e**, both of which were predicted to be sterically more congested than trifluoro analogue **3b** in modeling studies. These two analogues were poorly active, suggesting increased steric congestion by ring A, which did not allow the molecule to be properly accommodated into the hydrophobic pocket. Compound **3d** was also docked into the ATX crystal structure and a dramatically different orientation was observed in concert with our experimental findings (**Figure 3B**). Top poses of **3b** and **3d** showed good volume overlap but **3d** ran in the opposite direction and central aromatic ring B was twisted completely out of conjugation with the amide linker. This represents a very high energy conformation and unlikely to bind because of the conformational energy penalty. Next, we tested the effects of combining two different kinds of ring A substituents on the inhibitory activity of the molecule. We synthesized 3,5-difluoro-4-chloro analogue (**3f**) and the 3,5-dichloro-4-fluoro analogue (**3g**) and tested them for the ATX inhibition. Both analogues were highly potent ATX inhibitors with IC_{50} values of 83 nM and 40 nM, respectively. When docked to ATX, **3f** and **3b** adopted similar poses, with the electronegative chlorine in **3f** and the fluorine in

3b exposed to water in hydrophobic tunnel (**Figure 3**C). However, **3g** (not shown) adopted a completely different pose in which the halogenated aromatic A ring was in the hydrophobic pocket not in the hydrophobic tunnel, whereas the polar ends of the molecules overlapped, although running in opposite directions. Distances between the chlorine atoms of **3g** in the hydrophobic pocket predicted a water-mediated hydrogen bond with backbone atoms of L214 or A218 and a weak hydrogen bond with W276, which can be the reason for the two-fold higher potency of **3g** over **3 f**.

In an attempt to introduce more polar substituents into ring A, we prepared the 3,5-difluoro-4-cyano analogue (**3h**) and the 3,5,-difluoro 4-methyl ester analogue (**3i**). ATX activity measurements with these compounds showed that **3h** although modestly tolerated, **3i** was much less potent than **3** with IC_{50} values of 190 nM and 863 nM, respectively. Next, we hydrolyzed the ester bond in **3i** to the corresponding carboxylic acid and found that this new compound **4** was inactive.

1.2. Modifications of the linker between rings A and B. Subsequent synthetic modifications were aimed at the replacement of the amide bond of **3** to explore the importance of amide linker in ATX inhibition and to improve biological stability to amidases. To accomplish this, we first tried to synthesize the tri-fluoro benzoxazole (**6)** from intermediate **5** (**Scheme 2**). Although, intermediate **5** was obtained in good yield (76%) following the same strategy as shown in **scheme 1**, the synthetic procedure failed to turn intermediate **5** into desired oxazole **6**. An alternative strategy was applied to generate the oxazole **7** and the imidazole **8** using commercially available amino-phenol and amino-aniline precursors, respectively (**Scheme 2**). We also synthesized the N-methyl analogue (**9**). The four compounds **5**, **7**, **8**, and **9** obtained with the

synthetic route shown in **scheme 2** were tested for ATX inhibition (**Table 1**). Compound **5** showed potent ATX inhibition (IC_{50}=18 ± 2 nM), although less potent than the tri-fluoro compound **3b**. Compounds **7** and **8** closely mimic the amide framework, yet failed to inhibit ATX. It is noteworthy that the A and B aromatic rings in compounds **7** and **8** were predicted to be closer to planar than in the compounds with amide linkers. Additionally, compound **9** showed only very weak potency inhibiting ATX. We next examined the role of the carbonyl oxygen/carbonyl bond for the ATX inhibitory activity, because the SAR of the analogues we synthesized to this point indicated that the orientation of ring A relative to ring B around amide linkage is critical for the activity. To achieve this, we reduced amide bonds of the two most active ATX inhibitors, **3a** and **3b** (**Scheme 3**). The desired amines **10** and **11**, were obtained in good yields and were subjected to ATX inhibition analysis to find that the inhibitory activity of 3,4,5-trifluoro amine (**11**) was dramatically reduced relative to **3b** (IC_{50} = 395 nM *versus* 9 nM, **Table 1**). The di-fluoro amine **10** was found inactive.

In the next phase of our SAR analysis, we prepared compounds with thioamide linkers because of their higher stability against proteases compared to amides. We selected the four most potent inhibitors and synthesized the corresponding thioamides utilizing the synthetic strategy shown in **scheme 4**.[26] ATX inhibition assays showed that compounds **12,13, 14**, and **15** retained similar inhibitory activity to the amide analogues (**Table 1**). We also replaced the amide linker with a sulfonamide **(Scheme 5**).[27-30] The intermediate **18** was obtained in good yield and was converted into two different kinds of sulfonamides. Compounds **19** and **20** have the sulfonamide nitrogen linked to the ring B whereas, in compounds **22** and **23** the sulfonamide nitrogen is linked to ring A. All four

compounds lost their ATX inhibitory activity as shown in **Table 1**. These results underline the importance of linker geometry for ATX inhibition.

1.3. Modifications of the linker between ring B and C. Because these findings identified the importance of the amide-bond linkage for the inhibitory activity, we decided to further explore variations of the sulfonamide linkage between rings B and C to assess the role of the sulfonyl group. First, we replaced the sulfonamide linkage with a polar but smaller linkage keeping the morpholine ring intact. Additionally, we avoided the introduction of chirality in linking ring B to C. We constructed the hydrazine moiety, where the sulfonyl is replaced by a nitrogen atom as shown in **Scheme 6**. Compound **25** was obtained through intermediate **24** using the Buchwald-Hartwig cross-coupling reaction following the synthetic tools described by Cacchi et al.[31] Compound **25** completely lost ATX inhibitory activity (**Table 1**). This result confirms that the sulfonyl linkage provides a better contact with the polar surface of the ATX substrate binding pocket and forms some electrostatic interactions to promote strong binding. We hypothesized that introduction of a mesyl group (**26**) on the hydrazine in compound **25** could be as effective as compound **3b**, in contacting the polar enzyme surface. Many attempts to obtain **26b** remained unsuccessful.[32-34] However, utilizing excess sodium *tert*-butoxide and 1:11 ratio of methane sulfonyl chloride, compound **26a** was obtained. Testing revealed that compound **26a** was inactive, once again reinforcing the importance of the linker geometry. We also replaced ring C with N-methyl-piperazine shown in **Scheme 7**. The rationale behind this modification was that it would be more water soluble than the morpholine analogues. We selected the two most potent morpholine analogues **3b** and **3g**, and prepared their N-methyl piperazine analogues

28a and **28b**, following the synthetic strategy shown in **Scheme 7**. Analogues, **28a** and **28b**, were tested for ATX inhibition and found to inhibit the ATX with IC_{50} values of 66 nM and 55 nM, respectively (**Table 1**). Finally, we selected the more potent analogue **28b**, and converted it into the corresponding thioamide (**29**) which showed a potency of IC_{50}= 100 nM.

2. Pharmacological characterization of the benzene sulfonamide ATX Inhibitors

ATX has dual nucleotide pyrophosphate phosphatase and lysophosholipase D activity that can be selectively measured using the pNP-TMP and FS-3 substrates, respectively.[2, 13, 16] The inhibitory activities of the new compounds against the two different substrates are listed in **Tables 1**. Our primary test was to assess the inhibitory action of the new compounds on the lysophospholipase D activity of purified recombinant human ATX. Compound **3b** was found to be the most potent ATX inhibitor with an IC_{50} of ~ 9 nM in this assay. The mechanism of action was competitive; however, the traditional measure of a competitive inhibitor may not be appropriately applied in this context. **3b** inhibited hydrolysis of the lipid-like substrate FS-3 while sparing effects on hydrolysis of the nucleotide substrate pNP-TMP. Molecular modeling predicted that **3b** does not bind at the active site in which case both substrates would be affected. However, because the compound is targeted toward the hydrophobic pocket of ATX, it shares space with the binding site for the hydrophobic tail of lipid-like substrates like FS-3. As such, the mechanism of action presents itself as “competitive” in the FS-3 hydrolysis assay even though the binding site of the **3b** exists outside the

catalytic site of the enzyme. This particular behavior of ATX inhibitors has been noted before.[16]

3. Selective dose-dependent inhibition of LPA_1 GPCR by compounds 3b, 3f, and 3g

The product of ATX, LPA is ligand to at least six GPCRs and the benzene sulfonamide compounds we have generated in this study could also possess some ligand activity at the different LPAR subtypes. For this reason, we tested all new chemical entities with useful ATX inhibitory potency (< 250 nM) for agonist and antagonist activity at $LPA_{1/2/3/4/5}$ using cells stably transfected with each individual GPCR [35]. None of the compounds tested exhibited agonist activity at any of these LPA receptor subtypes. Additionally, of those screened, only **3b, 3f,** and **3g** exhibited antagonist activity, and this inhibition was specific to the LPA_1 receptor (**Table 2**, **Figure 4**). Compounds **3b** (ATX IC_{50} = 9 nM, LPA1 IC_{50} ~ 14 μM), **3f** (ATX IC_{50} = 83 nM, LPA1 IC_{50} ~ 6 μM)**,** and **3g** (ATX IC_{50} = 40 nM, LPA1 IC_{50} = 18 μM), were dual inhibitors of both ATX and the LPA_1 receptor.

4. Effect of benzene sulfonamide ATX Inhibitors on other members of the ENPP family

ATX constitutes one of three members of the ENPP family, comprised also of ENPP6 and ENPP7. Both ENPP6 and ENPP7 retain similar phosphodiesterase activity to ATX but lack its hydrophobic pocket. To test the inhibitory effects of benzene sulfonamide

ATX inhibitors versus purified recombinant ENPP6 and ENPP7, the nucleotide substrate p-nitrophenylphosphorylcholine (pNPPC) was used. None of the compounds tested exhibited inhibitory activity for ENPP6 or ENPP7 (data not shown) as the benzene sulfonamide structures are targeted to the hydrophobic pocket of ATX, which is not found in either of the other ENPP family members.

5. Inhibition of ATX-mediated invasion of A2058 human melanoma *in vitro*

We utilized the Boyden chamber assay to assess the effect of benzene sulfonamide analogues **3a**, **3b, 3f** and **14** on invasion of A2058 human melanoma cells *in vitro*. The A2058 cells invade the matrigel layer in an LPA-dependent manner. Therefore, we used exogenous LPC and recombinant ATX as a source of LPA. First, we screened the compounds at 10μM concentration alongside (4-pentadecylbenzyl)phosphonic acid [**30** (BMP22)][13], a potent ATX inhibitor that we have previously identified and characterized.[13] We found that all four inhibitors were as effective as **30** in inhibiting A2058 cell invasion across the matrigel layer in response to exogenous LPC and recombinant ATX (**figure 5A**). Subsequently, we generated dose response curves for compounds **3a**, **3b, 3f,** and **14** (**figure 5B**). All four inhibitors dose-dependently decreased the A2058 cell invasion with similar potencies (**Table 3**).

6. *In Vitro* Stability Analysis

The lead **3**, **3b**, **3f**, and **14** were analyzed for stability in the presence of cells in culture using liquid chromatography mass spectrometry. All analogs tested showed significant stability over the 40h of exposure to 4T1 cells in serum free culture medium. The lead, **3** maintained 79.7 ± 7.8% (16h) and 79.5 ± 12.6% (40h) of the 0h control signal. Whereas

the poly-halogenated amide and thioamide analogs appear to be a bit more stable in this system over this limited time course (**3b** maintained 102.6 ± 2.6% (16h) and 105.3 ± 2.7% (40h), **3f** 101.3 ± 3.7% (16h) and 108.2 ± 1.3%, and the thioamide **14** 93.2 ± 20.4% (16h) and 102.0 ± 14.5% (40h) of their corresponding 0h controls).

7. Inhibition of B16 murine melanoma lung metastasis by benzene sulfonamide ATX Inhibitors

To complement our *in vitro* invasion studies, we tested the effect of **3b** and **14** in the B16 lung metastasis *in vivo* model. We found that daily administration of compounds **3b** and **14** for a total of 10 days significantly reduced the number of metastatic lung nodules formed in mice (**Figure 6**).

8. Sensitization of therapy resistant 4T1 murine breast carcinoma cells and stem cell-like cells (CSC) to paclitaxel by benzene sulfonamide ATX Inhibitors

To further characterize the three most potent compounds, we tested them on the viability and growth of 4T1 murine breast cancer cells (**Figure 7**). Adherent cultures of 4T1 cells were treated for 24h with a range of 0-10 μM compounds **3b**, **3f**, **14**, or reference inhibitor **30** in RPMI with 1% (v/v) charcoal-stripped FBS. After 48h treatment with daily replenishment of inhibitor, cell number/viability was assessed (**Figure 7A**). Only **30** inhibited cell growth at 3 μM, whereas all other compounds failed to cause a significant reduction in cell number. However, unlike the other compounds, **14** was toxic at 10μM, the highest concentration tested.

LPA and ATX increase the resistance of cancer cells to chemo- and radiation therapy.[6] To assess whether the new ATX inhibitors could overcome chemoresistance, the 4T1

breast cancer cell line was exposed to increasing concentration of paclitaxel (PT) for 48h with or without 24h pre-treatment with 3 μM of compound **3b** or **3f**. Both ATX inhibitors caused a significant shift in the LD_{50} of PT dose-response relationship indicating that ATX inhibitor treatment made them more sensitive to PT (**Figure 7B**). The PT LD_{50} for reducing cell growth by 50% was 202 nM when applied alone. In contrast, the **3b** and **3f** reduced the LD_{50} to PT to 127 and 66 nM, respectively.

Next, we evaluated if these inhibitors were able to overcome chemoresistance to PT in cancer stem-like cells. To do this, we generated a paclitaxel-resistant 4T1 cell line (4T1-TaxR) and grew them in an anchorage-independent environment to induce sphere formation. This culture method has been widely used to enrich for breast CSC. We found that both **30** and compound **3b** were able to further reduce cell viability by ~25 to 30% compared to PT alone, suggesting that the ATX inhibitors were able to resensitize the CSC to PT treatment (**Figure 7C**).

Discussion and Conclusion

Here we report on the synthesis of ATX inhibitors that are benzene-sulfonamide analogues derived from hit compound **3** which, we identified via *in silico* screening of the Genome Research Institute library at the University of Cincinnati Drug Discovery Center.[2, 16] The parent compound **3**, although a potent non-lipid ATX inhibitor with an IC_{50} value ~ 117 nM, lacked sufficient stability and activity in cellular and *in* vivo assays. Thus, our study objectives were: 1) To improve the potency of ATX inhibition with IC_{50} values in the low nanomolar range and 2) Obtain compounds that were effective in *in* vitro cell-based assays and *in* vivo metastasis model dependent on ATX activity. We

have conducted four different kinds of SAR explorations of the **3** scaffold. The structural features explored included 1) modification of ring A substituents, 2) modification of the amide bond A-B ring linker, 3) modification of sulfonyl B-C ring linker, and 4) the modification of the ring C. The A-ring optimization has resulted in a number of substantially more active ATX inhibitors, including inhibitor **3b** (IC_{50} = 9 nM) and **5** (IC_{50} = 18 nM). When tested for agonist action at $LPA_{1/2/3/4/5}$ GPCR none of the compound were active up to 10μM, the highest concentration tested. However, three of the potent ATX inhibitors, **3b**, **3f**, and **3g**, were also effective in antagonizing the LPA_1-elicited Ca^2 responses. The antagonist potency of these ATX inhibitors was in the low micromolar range that is not negligible when assessing their cellular actions. Our synthetic improvement to increase the LPA_1 antagonist activity of derivatives of compounds **3b** and **3f** without compromising their low nanomolar ATX inhibitory activity were unsuccessful.

Unexpectedly, inhibition of ATX was highly sensitive to transformations of the amide linkage as any alteration led to deterioration of potency. Thioamides, including compound **14** (IC_{50} = 35 nM) were the most potent in this series, with three-fold better potency than the screening hit **3**. This finding underlines the importance of linker geometry for inhibition of ATX. The third optimization, was modification of the sulfonyl bond and this did not yield any compound that was more potent than **3**. Finally, replacement of morpholine with piperazine, was tolerated resulting in three more active compounds than the starting scaffold, the most potent **28b** showing an IC_{50} of 55 nM. It is noteworthy that the piperazine series with Log P values around 3.5 are water soluble.

We selected the three most potent amide analogues (**3a**, **3b, and 3f**) and the most potent thioamide analogue (**14**) in cellular assays using the ATX-dependent invasion of A2058 human melanoma cells *in vitro*. All four inhibitors showed good in vitro stability and dose-dependently decreased A2058 cell invasion with overlapping potencies (**Table 3**). In addition, two of these inhibitors, **3b** and **14** were shown to be effective in reducing the metastasis of B16F10 cells to the lungs of C57BL/6 mice. Compounds **30** and **3b** effectively resensitize the resistant 4T1 cell line (4T1-TaxR) to paclitaxel treatment. Our results complement the findings of Venkatraman et al., in which activation of the LPA_1 receptor promotes chemoresistance in breast cancer cells in part via the stabilization of Nrf2 and the subsequent increase in the transcription of various genes involved in drug resistance.[36] Thus compounds that have both inhibitory actions against ATX and LPA_1, might have therapeutic utility as adjuvant for the treatment of therapy resistant cancers.

In summary, this series of inhibitors meets the four objectives of our synthetic campaign as they lack carboxylic acid functionality, contain no chiral center, their molecular weight is less than 500 D, and each has IC_{50} values less than 85 nM for the ATX. During our study, Galapagos Inc., has developed a number of potent compounds with structural similarity to **3**, (**Figure 1A**).[1] One of the Galapagos compound has been reported to successfully complete the first in-human phase one clinical trial[1] giving us hope that our inhibitors will yield similar outcome with higher potency than Galapagos compound.

Galapagos

Experimental.

Chemistry.

General methods: All non-aqueous reactions were performed in oven-dried glassware under an inert atmosphere of dry nitrogen. All the reagents and solvents were purchased from Aldrich (St. Louis, MO), Alfa-Aesar (Ward Hill, MA), Combi-Blocks (San Diego, CA), Ark Pharm (Libertyville, IL) and used without further purification. Analytical thin-layer chromatography was performed on Silica Gel GHLF 10 x 20 cm Analtech TLC Uniplates (Analtech, Newark, DE) and were visualized by fluorescence quenching under UV light. Biotage SP1 Flash Chromatography Purification System (Charlotte, NC) (Biotage SNAP Cartridge, silica, 50g & 100g) was used to purify the compounds. 1H NMR and 13C NMR spectra were recorded on a Varian Inova-500 spectrometer (500 MHz) (Agilent Technologies, Santa Clara, CA) or a Bruker Ascend 400 (400 MHz) (Billerica, MA) spectrometer. Chemical shifts are reported in ppm on the δ scale and referenced to the appropriate solvent peak. Mass spectra were collected on a Brucker ESQUIRE electrospray/ion trap instrument in the positive and negative modes. High resolution mass spectrometer (HRMS) data were acquired on a Waters Xevo G2-S QTOF (Milford, MA) system equipped with an Acquity I-class UPLC system. Purity of all tested compounds was determined to be >95% as evident by ^{1}H NMR and HPLC. HPLC method used to determine purity is as follows: Compound purity was analyzed using Agilent 1100 HPLC system (Santa Clara, CA) with a Zorbax SB-C18 column, particle size 3.5 µm, 4.6 × 150 mm from Agilent. Mobile phases consist of water with 0.1% formic acid (A) and acetonitrile with 0.1% formic acid (B). Flow rate of 1 mL/min was used. The gradient elution started at 50% B. It reached at 100% B from 0 to 9 min and was maintained at it from 9 to 12 min, and was then decreased to 50% B from 12 to

15 min and stopped. Compound purity was monitored with a DAD detector set at 254 nm.

Synthesis of 2,4-dichloro-5-(chlorosulfonyl)benzoic acid (1). To a cooled (0 ^{O}C) chlorosulfonic acid (10.4 mL, 157 mmol) 2,4-dichlorobenzoic acid (5 g, 26 mmol) was added potion wise. The reaction mixture was subsequently heated to 140 ^{O}C and continued to stir for 16 hrs. The reaction mixture was cooled to room temperature and poured into crushed ice. The formed white precipitates were collected by filtration and dried under the vacuum. Yield = 80%. The characterizations comply with the literature.[37]

General procedure for the Synthesis of compounds 2 and 27. To a solution of **1** (3g, 10.3 mmol) in 20 mL CH_2Cl_2, trimethylamine was added (3.61 mL, 26 mmol). The reaction mixture was cooled down to 0 ^{O}C under the ice. The corresponding secondary amine (11.4 mmol) was added drop-wise and the reaction mixture was continued to stir over the night. The reaction mixture was concentrated and the crude was taken for next step without further purification.

General procedure for the Synthesis of compounds 3 as well as 3a to 3i. To a solution of compound **2** (0.46g, 1.4 mmol) in 20 mL of CH_2Cl_2, a volume of 1 mL $SOCl_2$ (13.6 mmol) and 2 drops of DMF were added under argon atmosphere. The reaction was continued to stir at room temperature over the night. The reaction mixture was concentrated and dissolved back again in 20 mL CH_2Cl_2. Pyridine (330 uL, 4.1 mmol) and the corresponding aniline (1.2 mmol) were added under argon atmosphere. The reaction mixture was allowed to stir over the night at room temperature. The reaction mixture was extracted with 10% HCl, water, and brine solution. The organic layer was

dried over $MgSO_4$, concentrated, and purified by column chromatography leading to the pure product.

2,4-Dichloro-*N*-(3-fluorophenyl)-5-(morpholinosulfonyl)benzamide (**3**). The compound **3** was prepared following general procedure for the synthesis of **3** as well as **3a**-**3i**. The crude was purified in 1% MeOH/CH_2Cl_2 yielding the pure product as white solid. Yield = 70%. ^{1}H NMR (400 MHz, DMSO-d_6) δ 10.94 (s, 1H), 8.18 (d, *J* = 3.8 Hz, 2H), 7.77 – 7.67 (m, 1H), 7.53 – 7.37 (m, 2H), 7.12 – 6.95 (m, 1H), 3.69 (t, *J* = 4.70 Hz, 4H), 3.28 (t, *J* = 5.0 Hz, 4H). HRMS [$C_{17}H_{16}N_2O_4FSCl_2^+$]: calcd 433.0192, found 433.0182.

2,4-Dichloro-*N*-(3,4-difluorophenyl)-5-(morpholinosulfonyl)benzamide (3a). The compound **3a** was prepared following general procedure for the synthesis of **3** as well as **3a**-**3i**. The crude was purified in 1% MeOH/CH_2Cl_2 yielding the pure product as white solid. Yield = 72%. mp = 221.3 ^{O}C. ^{1}H NMR (400 MHz, DMSO) δ 10.90 (s, 1H), 8.13 (s, 2H), 7.85 (ddd, *J* = 12.8, 7.4, 2.4 Hz, 1H), 7.45 (ddd, *J* = 27.0, 18.1, 9.0 Hz, 2H), 3.63 (t, *J* = 4.46, 4H), 3.22 (t, *J* = 4.77, 4H). ^{13}C NMR (101 MHz, DMSO) δ 162.71, 135.72, 135.29, 134.19, 133.20, 133.10, 131.49, 117.76, 117.58, 116.22, 109.00, 108.79, 65.72, 45.49. HRMS [$C_{17}H_{15}N_2O_4F_2SCl_2^+$]: calcd 451.0098, found 451.0099.

2,4-Dichloro-5-(morpholinosulfonyl)-*N*-(3,4,5-trifluorophenyl)benzamide (3b). The compound **3b** was prepared following general procedure for the synthesis of **3** as well as **3a**-**3i**. The crude was purified in 1% MeOH/CH_2Cl_2 yielding the pure product as white solid. Yield = 71.5%. mp = 237.8 ^{O}C. ^{1}H NMR (400 MHz, DMSO) δ 11.05 (s, 1H), 8.15 (d, *J* = 2.1 Hz, 2H), 7.58 (dd, *J* = 9.9, 6.5 Hz, 2H), 3.63 (t, *J* = 4.67, 4H), 3.22 (t, *J* = 4.53, 4H). ^{13}C NMR (101 MHz, DMSO) δ 162.99, 135.70, 134.94, 134.27, 133.42,

133.17, 131.53, 104.39, 104.15, 65.72, 45.49. HRMS [$C_{17}H_{14}N_2O_4F_3SCl_2^+$]: calcd 469.0003, found 451.0012.

2,4-Dichloro-5-(morpholinosulfonyl)-*N*-(perfluorophenyl)benzamide (3c). The compound **3c** was prepared following general procedure for the synthesis of **3** as well as **3a**-**3i**. The crude was purified in 1% MeOH/CH_2Cl_2 yielding the pure product as white solid. Yield = 65%. mp = 237.1 ^{O}C. ^{1}H NMR (400 MHz, DMSO-d_6) δ 11.01 (s, 1H), 8.15 (dd, *J* = 24.5, 19.0 Hz, 2H), 3.70 – 3.55 (m, 4H), 3.27 – 3.13 (m, 4H). ^{13}C NMR (101 MHz, DMSO-d_6) δ 166.95, 163.05, 136.00, 134.33, 133.82, 133.46, 131.49, 65.73, 45.43. HRMS [$C_{17}H_{12}N_2O_4F_5SCl_2^+$]: calcd 504.9815, found 504.9838.

2,4-Dichloro-5-(morpholinosulfonyl)-*N*-(3,4,5-trichlorophenyl)benzamide (3d). The compound **3d** was prepared following general procedure for the synthesis of **3** as well as **3a**-**3i**. The crude was purified in 1% MeOH/CH_2Cl_2 yielding the pure product as white solid. Yield = 75%. mp = 303.0 ^{O}C. ^{1}H NMR (400 MHz, DMSO-d_6) δ 11.09 (s, 1H), 8.18 (s, 1H), 8.15 (s, 1H), 7.94 (s, 2H), 3.68 – 3.57 (t, J = 4.32, 4H), 3.27 – 3.16 (t, J = 4.84, 4H). ^{13}C NMR (101 MHz, DMSO-d_6) δ 163.10, 138.36, 135.74, 134.78, 134.30, 133.52, 133.20, 133.01, 131.59, 124.51, 119.89, 65.72, 45.48. HRMS [$C_{17}H_{14}N_2O_4SCl_5^+$]: calcd 516.9117, found 516.9108.

2,4-Dichloro-5-(morpholinosulfonyl)-*N*-(3,4,5-trimethoxyphenyl)benzamide (3e). The compound **3e** was prepared following general procedure for the synthesis of **3** as well as **3a**-**3i**. The crude was purified in 1% MeOH/CH_2Cl_2 yielding the pure product as white solid. Yield = 65%. mp = 281.2 ^{O}C. ^{1}H NMR (400 MHz, Chloroform-*d*) δ 8.34 (s, 1H), 7.83 (s, 1H), 7.66 (s, 1H), 6.93 (s, 2H), 3.89 (s, 6H), 3.84 (s, 3H), 3.73 (dd, *J* = 5.9,

3.7 Hz, 4H), 3.39 – 3.18 (m, 4H). HRMS [$C_{20}H_{23}N_2O_7SCl_2^+$]: calcd 505.0603, found 505.0606.

2,4-Dichloro-*N*-(4-chloro-3,5-difluorophenyl)-5-(morpholinosulfonyl)benzamide (3f). The compound **3f** was prepared following general procedure for the synthesis of **3** as well as **3a**-**3i**. The crude was purified in 1% MeOH/CH_2Cl_2 yielding the pure product as white solid. Yield = 75%. mp = 275.7 ^{O}C. ^{1}H NMR (400 MHz, DMSO-d_6) δ 11.17 (s, 1H), 8.16 (d, *J* = 6.1 Hz, 2H), 7.60 (d, *J* = 9.1 Hz, 2H), 3.63 (t, J = 4.35, 4H), 3.22 (t, J = 4.93, 4H). ^{13}C NMR (101 MHz, $CDCl_3$) δ 168.38, 140.96, 140.08, 139.55, 138.75, 138.43, 136.82, 109.16, 108.89, 70.97, 50.74. HRMS [$C_{17}H_{14}N_2O_4F_2SCl_3^+$]: calcd 484.9708, found 484.9729.

2,4-Dichloro-*N*-(3,5-dichloro-4-fluorophenyl)-5-(morpholinosulfonyl)benzamide (3g). The compound **3g** was prepared following general procedure for the synthesis of **3** as well as **3a**-**3i**. The crude was purified in 1% MeOH/CH_2Cl_2 yielding the pure product as white solid. Yield = 76%. mp = 297.4 ^{O}C. ^{1}H NMR (400 MHz, DMSO-d_6) δ 11.00 (s, 1H), 8.16 (d, *J* = 9.9 Hz, 2H), 7.85 (d, *J* = 6.1 Hz, 2H), 3.63 (t, *J* = 4.8 Hz, 4H), 3.22 (t, J = 5.22 Hz, 4H). ^{13}C NMR (101 MHz, DMSO-d_6) δ 162.96, 135.74, 134.89, 134.28, 133.45, 133.18, 131.56, 121.11, 120.93, 120.19, 65.72, 45.49. HRMS [$C_{17}H_{14}N_2O_4FSCl_4^+$]: calcd 500.9412, found 500.9409.

2,4-Dichloro-*N*-(4-cyano-3,5-difluorophenyl)-5-(morpholinosulfonyl)benzamide (3h). The compound **3h** was prepared following general procedure for the synthesis of **3** as well as **3a**-**3i**. The crude was purified in 1% MeOH/CH_2Cl_2 yielding the pure product as white solid. Yield = 72%. mp = 240.7 ^{O}C. ^{1}H NMR (400 MHz, DMSO) δ 11.51 (s, 1H), 8.19 (d, *J* = 17.4 Hz, 2H), 7.63 (d, *J* = 10.1 Hz, 2H), 3.63 (t, *J* = 4.75 Hz, 4H), 3.22 (t, *J* =

4.68, 4H). ^{13}C NMR (101 MHz, DMSO-d_6) δ 163.67, 135.69, 134.51, 134.36, 133.73, 133.23, 131.69, 109.75, 103.18, 102.93, 65.72, 45.48. HRMS [$C_{18}H_{14}N_3O_4F_2SCl_2^+$]: calcd 476.0050, found 476.0048.

Methyl 4-(2,4-dichloro-5-(morpholinosulfonyl)benzamido)-2,6-difluorobenzoate (3i). The compound **3i** was prepared following general procedure for the synthesis of **3** as well as **3a**-**3i**. The crude was purified in 1% MeOH/CH_2Cl_2 yielding the pure product as white solid. Yield = 69%. mp = 216.4.1^{O}C. ^{1}H NMR (400 MHz, DMSO-d_6) δ 11.29 (s, 1H), 8.17 (d, *J* = 14.8 Hz, 2H), 7.50 (d, *J* = 10.6 Hz, 2H), 3.87 (s, 3H), 3.63 (t, J = 4.46 Hz, 4H), 3.23 (t, J = 4.69 Hz, 4H). ^{13}C NMR (101 MHz, DMSO-d_6) δ 163.37, 160.85, 143.00, 135.70, 134.69, 134.34, 133.61, 133.19, 131.63, 103.16, 102.90, 65.72, 52.70, 45.49. HRMS [$C_{19}H_{17}N_2O_6F_2SCl_2^+$]: calcd 509.0152, found 509.0146.

4-(2,4-Dichloro-5-(morpholinosulfonyl)benzamido)-2,6-difluorobenzoic acid (4). An amount of 8.5 mg LiOH (0.35 mmol) was added to a solution of compound **3i** (90 mg, 0.17 mmol) in 10 THF/ MeOH (2: 1) mixture. The reaction mixture was allowed to stir over the night at room temperature. The reaction mixture was diluted with water, acidified with 10% HCl (pH = 4), extracted with ethyl acetate. The organic layer was dried over $MgSO_4$ and purified through flash chromatography (2% MeOH/CH_2Cl_2) leading to the pure product as white solid. Yield = 62%. mp = 256.2 ^{O}C. ^{1}H NMR (400 MHz, DMSO-d_6) δ 13.63 (s, 1H), 10.73 (s, 1H), 8.12 (s, 1H), 7.57 (s, 1H), 7.52 (d, *J* = 10.4 Hz, 2H), 4.01 (s, 3H), 3.62 (t, *J* = 4.66 Hz, 4H), 3.14 (t, *J* = 4.51 Hz, 4H). ^{13}C NMR (101 MHz, DMSO-d_6) δ 163.12, 161.79, 159.94, 135.47, 132.99, 126.54, 123.22, 116.17, 103.04, 102.74, 65.67, 57.40, 45.50. HRMS [$C_{19}H_{18}N_2O_7F_2SCl^+$]: calcd 491.0491, found 491.0500.

***N*-(2-Bromo-3,4,5-trifluorophenyl)-2,4-dichloro-5-(morpholinosulfonyl)benzamide (5)**. The compound **5** was prepared following general procedure for the synthesis of **3** as well as **3a**-**3i**. The crude was purified in 1% MeOH/CH_2Cl_2 yielding the pure product as white solid. Yield = 76%. mp = 196.1 ^{O}C. ^{1}H NMR (400 MHz, DMSO-d_6) δ 10.64 (s, 1H), 8.21 (s, 1H), 8.12 (s, 1H), 7.86 (m, 1H), 3.64 (t, *J* = 4.7 Hz, 4H), 3.23 (t, *J* = 4.7 Hz, 4H). ^{13}C NMR (101 MHz, DMSO-d_6) δ 163.37, 135.82, 134.80, 134.02, 133.29, 133.07, 131.77, 111.61, 65.71, 45.46. HRMS [$C_{19}H_{17}N_2O_6F_2SCl_2^+$]: calcd 546.9109, found 546.9113.

2-(2,4-Dichloro-5-(morpholinosulfonyl)phenyl)-7-fluorobenzo[d]oxazole (7). To a solution of 0.28g of compound **2** (0.82 mmol) in 20 mL of CH2Cl2, was added a volume of 0.6 mL $SOCl_2$ (8.2 mmol) and catalytic amount of DMF (2 drops) under argon atmosphere. The reaction was allowed to sir for 12 hrs. The reaction mixture was concentrated and dissolved back in 20 mL CH2Cl2. A volume of 0.2 mL pyridine (2.5 mmol) as well as an amount of 0.105g (0.82 mmol) 2-amino-6-fluorophenol was added to the solution under argon atmosphere. The reaction mixture was allowed to stir over the night at room temperature. The reaction mixture was diluted with 20 mL CH2Cl2 and extracted with 10% HCl. The organic layer was dried over MgSO4 and concentrated. The crude was dissolved in 25 mL toluene. An amount of 156 mg p-TSA (0.82 mmol) was added to the solution under argon atmosphere. The reaction mixture was refluxed over 12 hrs. The reaction was cooled down to room temperature, poured into water and extracted with ethyl acetate. The organic layer was separated then washed with water, brine, dried ($MgSO_4$), filtered and concentrated. The crude product was purified by column chromatography (silica gel, 30% ethyl acetate/hexanes) to afford the desired

product as an off-white solid. Yield = 77%. mp = 167.4 ^{O}C. ^{1}H NMR (400 MHz, Chloroform-*d*) δ 8.87 (s, 1H), 7.80 (s, 1H), 7.66 (dd, *J* = 8.0, 0.9 Hz, 1H), 7.37 (td, *J* = 8.2, 4.6 Hz, 1H), 7.21 (ddd, *J* = 9.9, 8.3, 0.9 Hz, 1H), 3.90 – 3.62 (m, 4H), 3.49 – 3.20 (m, 4H). ^{13}C NMR (101 MHz, $CDCl_3$) δ 158.89, 148.30, 145.78, 144.63, 138.44, 137.84, 135.44, 134.80, 125.61, 124.72, 116.62 (d, *J* = 4.3 Hz), 113.09, 112.93, 66.51, 45.90. HRMS [$C_{17}H_{14}N_2O_4FSCl_2^+$]: calcd 431.0035, found 431.0045.

4-((2,4-Dichloro-5-(5,6-difluoro-1H-benzo[d]imidazol-2-yl)phenyl)sulfonyl)-morpholine (8). To a solution of 0.28g of compound **2** (0.82 mmol) in 20 mL of CH_2Cl_2, was added a volume of 0.6 mL $SOCl_2$ (8.2 mmol) and catalytic amount of DMF (2 drops) under argon atmosphere. The reaction was allowed to sir for 12 hrs. The reaction mixture was concentrated and dissolved back in 20 mL CH_2Cl_2. A volume of 0.2 mL pyridine (2.5 mmol) as well as an amount of 0.118g (0.82 mmol) 4, 5-difluorobenzene-1,2-diamine was added to the solution under argon atmosphere. The reaction mixture was allowed to stir over the night at room temperature. The mixture was diluted with dichloromethane (30ml) and washed with saturated aqueous sodium bicarbonate solution (80ml). The organic phase was dried over $MgSO_4$ and the solvent removed to provide the amide as a mixture of isomers. The crude amide was combined with phosphorus oxychloride (10ml) under an argon atmosphere, heated to reflux for 100 minutes, then allowed to cool down to room temperature. The mixture was poured into ice-water (100ml) and neutralized with 2N sodium hydroxide solution. Saturated aqueous sodium bicarbonate solution (60ml) was added and the aqueous phase was extracted with ethyl acetate (3 x 70ml). Water (150ml) was added to the combined organic phases and the pH was adjusted to 3 with 2N aqueous hydrochloric acid. The

organic layer was washed with brine (100ml), dried over $MgSO_4$and the solvent removed to give a brown solid. The crude was purified by flash chromatography (35% EtOAc/hexanes) to afford the desired product as light brown solid. Yield = 71%. mp = 175.2 ^{O}C. ^{1}H NMR (400 MHz, DMSO-d_6) δ 8.51 (s, 1H), 8.19 (s, 1H), 7.83 – 7.71 (m, 2H), 3.64 (t, *J* = 4.8 Hz, 5H), 3.24 (dd, *J* = 5.9, 3.6 Hz, 4H). ^{13}C NMR (101 MHz, DMSO-d_6) δ 148.55, 148.41, 146.18, 136.45, 134.30, 134.20, 133.91, 132.88, 128.32, 65.71, 54.87, 45.48. HRMS [$C_{17}H_{14}N_3O_3F_2SCl_2^+$]: calcd 448.0101, found 448.0106.

2,4-Dichloro-N-(3-fluorophenyl)-*N*-methyl-5-(morpholinosulfonyl)benzamide (9). The compound **9** was prepared following general procedure for the synthesis of **3** as well as **3a**-**3i**. The crude was purified in 1% MeOH/CH_2Cl_2 yielding the pure product as white solid. Yield = 75%. mp = 128.7 ^{O}C. ^{1}H NMR (400 MHz, DMSO-d_6) δ 8.16 – 7.72 (m, 2H), 7.47 – 7.24 (m, 2H), 7.22 – 6.99 (m, 2H), 3.57 (t, *J* = 4.6 Hz, 4H), 3.40 (s, 3H), 2.95 (bt, *J* = 5.2 Hz, 4H). ^{13}C NMR (101 MHz, DMSO-d_6) δ 164.16, 160.61, 144.17, 135.50, 135.09, 133.32, 133.03, 132.68, 132.05, 131.84, 130.86, 123.31, 114.57, 65.53, 45.47, 36.60. HRMS [$C_{18}H_{18}N_2O_4FSCl_2^+$]: calcd 447.0348, found 447.0369.

***N*-(2,4-Dichloro-5-(morpholinosulfonyl)benzyl)-3,4-difluoroaniline (10)**. To a solution of compound **3a** (0.15g, 0.33 mmol) in anhydrous THF (20 mL), a volume of 47 µL of BH_3.DMS (0.5 mmol) was added under argon atmosphere. The reaction mixture was allowed to reflux over 72 hrs and reaction progress was monitored by TLC. The reaction was quenched with 30 mL of water, extracted with ethyl acetate. The organic layer was extracted with brine and dried over $MgSO_4$. The crude was purified through flash chromatography (silica gel, 40% EtOAc/hexanes) providing access to the pure product as white solid. Yield = 75%. mp = 154.8 ^{O}C. ^{1}H NMR (400 MHz, $CDCl_3$) δ 7.89

(s, 1H), 7.53 (s, 1H), 6.96 – 6.79 (m, 1H), 6.33 – 6.10 (m, 2H), 4.35 (d, *J* = 6.0 Hz, 2H), 4.23 (t, *J* = 5.9 Hz, 1H), 3.58 (t, J = 4.44 Hz, 4H), 3.03 (t, *J* = 4.54 Hz, 4H). ^{13}C NMR (101 MHz, DMSO-d_6) δ 145.36, 137.86, 136.88, 133.19, 132.53, 131.01, 130.11, 117.66, 117.48, 108.10, 100.73, 100.53, 65.50, 45.45, 43.83. HRMS [$C_{17}H_{17}N_2O3F_2SCl_2^+$]: calcd 437.0305, found 437.0307.

***N*-(2,4-Dichloro-5-(morpholinosulfonyl)benzyl)-3,4,5-trifluoroaniline (11)**. To a solution of compound **3b** (0.15g, 0.32 mmol) in anhydrous THF (20 mL), a volume of 46 µL of BH_3.DMS (0.48 mmol) was added under argon atmosphere. The reaction mixture was allowed to reflux over 24 hrs and reaction progress was monitored by TLC. The reaction was quenched with 30 mL of water, extracted with ethyl acetate. The organic layer was extracted with brine and dried over $MgSO_4$. The crude was purified through flash chromatography (silica gel, 40% EtOAc/hexanes) providing access to the pure product as white solid. Yield = 72%. mp = 149.4 ^{O}C. ^{1}H NMR (400 MHz, $CDCl_3$) δ 7.89 (s, 1H), 7.54 (s, 1H), 6.16 – 5.94 (m, 2H), 4.31 (dd, *J* = 13.5, 5.0 Hz, 3H), 3.61 (t, *J* = 4.84 Hz, 4H), 3.08 (t, *J* = 5.0 Hz, 4H). ^{13}C NMR (101 MHz, DMSO) δ 152.26, 149.91, 144.61, 137.99, 136.42, 133.27, 132.60, 131.01, 130.33, 96.08, 95.84, 65.54, 45.47, 43.66. HRMS [$C_{17}H_{16}N_2O3F_3SCl_2^+$]: calcd 455.0211, found 455.0206.

General procedure for the synthesis of compounds from 12-15. To a solution of 0.2 g (1 equivalent) **3**, **3a**, **3b**, or **3g** in toluene (20 mL), was Lawesson's reagent (0.9 equivalent) under argon atmosphere as demonstrated in the literature.[26] The reaction was allowed to reflux over 12 hrs. The reaction was cooled down to room temperature. The solvent was evaporated and the crude was purified through flash chromatography (silica gel, 30%-35% EtOAc/hexanes) yielding the pure product as the light yellow solid.

2,4-Dichloro-*N*-(3-fluorophenyl)-5-(morpholinosulfonyl)benzothioamide (12). The compound **12** was obtained following the general procedure for the preparation of compounds **12**-**15**. The crude was purified through flash column (silica gel, 30% EtOAc/hexanes) leading to the pure product as the light yellow solid. Yield = 68%. mp = 181.0^{O}C. ^{1}H NMR (400 MHz, DMSO-d_6) δ 12.45 (s, 1H), 8.11 (s, 1H), 8.06 (dt, *J* = 11.4, 2.3 Hz, 1H), 8.00 (s, 1H), 7.71 – 7.64 (m, 1H), 7.53 (td, *J* = 8.2, 6.7 Hz, 1H), 7.19 (td, *J* = 8.5, 1.8 Hz, 1H), 3.65 (t, *J* = 4.64 Hz, 4H), 3.21 (t, J = 4.72 Hz, 4H). ^{13}C NMR (101 MHz, DMSO-d_6) δ 141.97, 133.92, 133.71, 132.78, 131.68, 131.18, 130.68, 130.59, 118.73, 109.48, 109.23, 65.68, 45.51. HRMS [$C_{17}H_{16}N_2O3FS_2Cl_2^+$]: calcd 448.9963, found 448.9956.

2,4-Dichloro-*N*-(3,4-difluorophenyl)-5-(morpholinosulfonyl)benzothioamide (13). The compound **13** was obtained following the general procedure for the preparation of compounds **12**-**15**. The crude was purified through flash column (silica gel, 32% EtOAc/hexanes) leading to the pure product as the light yellow solid. Yield = 70%. ^{1}H NMR (400 MHz, $CDCl_3$) δ 9.55 (s, 1H), 8.19 – 7.86 (m, 2H), 7.71-7.40 (m, 2H), 7.31 – 7.15 (m, 1H), 3.71 (bs, 4H), 3.23 (bs, 4H). ^{13}C NMR (101 MHz, $CDCl_3$) δ 192.37, 151.23 (d, *J* = 13.4 Hz), 150.07 (d, *J* = 12.8 Hz), 148.76 (d, *J* = 13.4 Hz), 147.58 (d, *J* = 12.7 Hz), 141.70, 134.58, 134.44, 133.99, 133.39, 132.76, 132.39, 119.40 (d, *J* = 2.4 Hz), 117.69, 117.50, 112.99, 112.78, 66.31, 45.87. HRMS [$C_{17}H_{15}N_2O_3F_2S_2Cl_2^+$]: calcd 466.9869, found 466.9869.

2,4-Dichloro-5-(morpholinosulfonyl)-*N*-(3,4,5-trifluorophenyl)benzothioamide (14). The compound **14** was obtained following the general procedure for the preparation of compounds **12**-**15**. The crude was purified through flash column (silica gel, 35%

EtOAc/hexanes) leading to the pure product as the light yellow solid. Yield = 71%. mp = 152.1 ^{O}C. ^{1}H NMR (400 MHz, $CDCl_3$) δ 9.41 (s, 1H), 8.05 (s, 1H), 7.68 (dd, *J* = 8.7, 6.2 Hz, 2H), 7.59 (s, 1H), 3.73 (t, *J* = 5.23 Hz, 4H), 3.25 (t, *J* = 5.23 Hz, 4H). ^{13}C NMR (101 MHz, $CDCl_3$) δ 191.63, 151.41, 140.50, 133.31, 133.21, 132.36, 132.08, 131.50, 106.82, 106.57, 65.33, 44.87. HRMS [$C_{17}H_{14}N_2O_3F_3S_2Cl_2^+$]: calcd 484.9775, found 484.9778.

2,4-Dichloro-*N*-(3,5-dichloro-4-fluorophenyl)-5-(morpholinosulfonyl)-benzothioamide (15). The compound **15** was obtained following the general procedure for the preparation of compounds **12**-**15**. The crude was purified through flash column (silica gel, 35% EtOAc/hexanes) leading to the pure product as the light yellow solid. Yield = 72%. mp = 175.2 ^{O}C. ^{1}H NMR (400 MHz, DMSO-d_6) δ 12.51 (s, 1H), 8.17 (d, *J* = 6.0 Hz, 2H), 8.11 (s, 1H), 8.05 (s, 1H), 3.65 (bt, *J* = 4.41 Hz, 4H), 3.21 (bt, *J* = 4.31 Hz, 4H). ^{13}C NMR (101 MHz, DMSO-d_6) δ 192.75, 152.43, 149.96, 141.53, 135.81 (d, *J* = 4.4 Hz), 134.01, 133.78, 132.83, 131.92, 131.20, 123.89, 121.07, 120.88, 65.68, 45.51. HRMS [$C_{17}H_{14}N_2O_3FS_2Cl_4^+$]: calcd 516.9184, found 516.9227.

2,4-Dichloro-5-nitrobenzene-1-sulfonyl chloride (16). Intermediate **16** was prepared following the experimental procedure for the preparation of intermediate **1** starting with 5g of 2,4-dichloro-1-nitrobenzene (26 mmol). An amount of 5.7g (19.6 mmol, 75%) pure product was obtained as off white solid upon drying under the vacuum. ^{1}H NMR (400 MHz, DMSO-d_6) δ 8.44 (s, 1H), 7.91 (s, 1H).

4-((2,4-Dichloro-5-nitrophenyl)sulfonyl)morpholine (17). Intermediate **17** was prepared following the general procedure for the preparation of intermediate **2** and **27** staring with 3.5g of intermediate **16** (12 mmol). An amount of 3.2g (9.3 mmol, 78%) pure

product was obtained as the off white solid. ^{1}H NMR (400 MHz, $CDCl_3$) δ 8.61 (s, 1H), 7.79 (s, 1H), 3.75 (t, *J* = 4.71 Hz, 4H), 3.35 (t, *J* = 4.31 Hz, 4H).

2,4-Dichloro-5-(morpholinosulfonyl)aniline (18). The nitro intermediate **17** (3g, 8.8 mmol) was dissolved in a mixture of EtOH and H_2O (40mL, 10:1). Powdered iron (2.25g, 35.2 mmol) and five drops of HCl (12 M) were added. The mixture was refluxed 5 hrs. The mixture was cooled to room temperature and the solvent was evaporated. HCl (1N, 100 mL) was added and the mixture was extracted with EtOAc (100 mL). The organic phase was extracted with brine, dried over MgSO4 and concentrated providing the pure product as the light red solid (2.6g, 8.3 mmol, 95%). ^{1}H NMR (400 MHz, DMSO-d_6) δ 7.58 (s, 1H), 7.41 (s, 1H), 6.04 (bs, 2H), 3.54 (t, *J* = 5.0 Hz, 4H), 3.13 (t, *J* = 4.86 Hz, 4H).

Synthesis of compound 19 and 20. To a solution of 0.2g **18** (0.64 mmol) in 15 mL CH_2Cl_2, was added Et_3N (267 µL, 1.9 mmol), 3-fluorobenzenesulfonyl chloride (0.149g, 0.77 mmol), and catalytic amount of DMAP under argon atmosphere. The reaction was allowed to stir at room temperature over 96 hrs and monitored by TLC. Reaction led to formation of two new spots as determined by TLC. The reaction mixture was diluted with 30 mL CH_2Cl_2. Organic layer was extracted with 10% HCl, H_2O, brine, and evaporated under reduced pressure. The crude with two spots were isolated by flash chromatography (silica gel, 30%~45% EtOAc/hexanes) providing pure compound **19** (yield = 33%) and **20** (yield = 60%) as white solids. Compound **19**. ^{1}H NMR (400 MHz, $CDCl_3$) δ 8.24 (s, 1H), 7.72 – 7.43 (m, 4H), 7.33 (tdd, *J* = 8.3, 2.5, 0.9 Hz, 1H), 3.74 (t, *J* = 5.10 Hz, 4H), 3.28 (t, *J* = 5.04 Hz, 4H). ^{13}C NMR (101 MHz, $CDCl_3$) δ 163.71, 161.19, 140.34 (d, *J* = 6.8 Hz), 135.81, 132.61, 132.43, 131.42 (d, *J* = 7.8 Hz), 129.09, 128.41,

123.97, 123.28 (d, *J* = 3.4 Hz), 121.42, 121.21, 114.94, 114.70, 66.47, 45.93. HRMS [$C_{16}H_{16}N_2O_5FS_2Cl_2^+$]: calcd 468.9862, found 467.9870. Compound **20**. ^{1}H NMR (400 MHz, $CDCl_3$) δ 7.90 – 7.37 (m, 10H), 3.73 (t, *J* = 4.86 Hz, 4H), 3.27 (t, *J* = 4.69 Hz, 4H). [$C_{22}H_{19}N_2O_7F_2S_3Cl_2^+$]: calcd 626.9699, found 626.9702.

2,4-Dichloro-5-(morpholinosulfonyl)benzene-1-sulfonyl chloride (21). The intermediate **21** was prepared from 1.5g (4.8 mmol) of intermediate **18** following the literature reported procedure.[32] An amount of 1.7g intermediate **21** (4.3 mmol, 90%) was obtained as the off white solid upon drying the precipitate under the vacuum. The product was taken for the next step.

General procedure for the formation of compound 22 and 23. To a solution of 0.2g **21** (0.51 mmol) in 15 mL of CH_2Cl_2, was added Et_3N 1.53 mmol) and appropriate aniline derivative (1.2 equivalent) under argon atmosphere. The reaction was allowed to stir at room temperature over 12 hrs. The reaction was diluted with 30 mL CH_2Cl_2, extracted with 10% HCl, H2O, and brine. The organic layer was dried over $MgSO_4$, concentrated under reduced pressure. The crude was purified through flash column (silica gel, 2% MeOH/CH_2Cl_2) yielding the pure product as off white solid.

2,4-Dichloro-*N*-(3-fluorophenyl)-5-(morpholinosulfonyl)benzenesulfonamide (22). Yield = 95%. mp = 170.7 ^{O}C. ^{1}H NMR (400 MHz, DMSO-d_6) δ 11.28 (s, 1H), 8.41 (s, 1H), 8.22 (s, 1H), 7.33 (dd, *J* = 15.0, 8.2 Hz, 1H), 7.01 – 6.77 (m, 3H), 3.59 (t, *J* = 4.23 Hz, 4H), 3.09 (t, J = 4.64 Hz, 4H). ^{13}C NMR (101 MHz, DMSO-d_6) δ 163.43, 161.0, 159.69, 138.36, 136.84, 136.21, 135.68, 135.42, 134.05, 133.34, 131.33, 131.24, 115.46, 111.25, 111.04, 106.59, 106.34, 65.60, 45.43. HRMS [$C_{16}H_{16}N_2O_5FS_2Cl_2^+$]: calcd 468.9861, found 468.9857.

2,4-Dichloro-5-(morpholinosulfonyl)-*N*-(3,4,5-trifluorophenyl)benzenesulfonamide (23). Yield = 94%. mp = 107.8 ^{O}C. ^{1}H NMR (400 MHz, Chloroform-*d*) δ 8.61 (s, 1H), 7.73 (s, 1H), 7.18 (bs, 1H), 6.90 – 6.70 (m, 2H), 3.76 – 3.65 (m, 4H), 3.31 – 3.17 (m, 4H). ^{13}C NMR (101 MHz, DMSO-d_6) δ 151.57, 149.06, 137.15, 136.19, 135.81, 135.12, 134.30, 133.34, 104.62, 104.55, 104.38, 65.63, 45.42. HRMS [$C_{16}H_{14}N_2O_5F_3S_2Cl_2^+$]: calcd 504.9673, found 504.9679.

5-Bromo-2,4-dichloro-*N*-(3,4,5-trifluorophenyl)benzamide (24). Intermediate **24** was prepared following the synthetic technique for the preparation of **3a**-**3i** starting with **2g** of 5-bromo-2,4-dichlorobenzoic acid (7.4 mmol). An amount of 2.22g (5.6%, 75%)

Pure **24** was obtained as a white solid upon purification through flash column (silica gel, 45% EtOAc/hexanes). ^{1}H NMR (400 MHz, Chloroform-*d*) δ 8.15 (s, 1H), 7.58 (s, 1H), 3.92 (s, 3H).

2,4-Dichloro-5-(morpholinoamino)-*N*-(3,4,5-trifluorophenyl)benzamide (25). Compound **25** was prepared from compound **24** (0.3g, 0.75 mmol) following the literature reported procedure of LiCl mediated palladium catalyzed coupling of hydrazine and phenyl bromide.[32] An amount of 0.195g (0.46 mmol, 62%) pure product was obtained as light yellowish solid upon purification through flash column (silica gel, 30% EtOAC/hexanes). mp = 196.1 ^{O}C. ^{1}H NMR (400 MHz, Chloroform-*d*) δ 7.95 (s, 1H), 7.65 (s, 1H), 7.51 – 7.29 (m, 3H), 5.15 (s, 1H), 3.81 (t, *J* = 4.6 Hz, 4H), 2.78 (bt, 4H). ^{1}H NMR (400 MHz, DMSO-d_6) δ 10.86 (s, 1H), 7.77 – 7.41 (m, 3H), 7.29 (s, 1H), 7.05 (s, 1H), 3.67 (t, *J* = 4.4 Hz, 4H), 2.79 (t, *J* = 4.7 Hz, 4H). ^{13}C NMR (101 MHz, DMSO-d_6) δ 165.16, 151.31, 148.88, 142.82, 135.57, 129.64, 117.71, 116.95, 112.40, 103.99, 103.75, 66.28, 54.47. HRMS [$C_{17}H_{15}N_3O_2F_3Cl_2^+$]: calcd 420.0493, found 420.0484.

2,4-Dichloro-*N*-(methylsulfonyl)-5-(morpholinoamino)-*N*-(3,4,5-trifluorophenyl)-benzamide (26a). To a solution of 0.1g of **25** (0.24 mmol) in DMSO, was added NaO^{t}Bu (0.069 g, 0.72 mmol) at 0 ^{O}C under argon atmosphere. Methanesulfonylchloride (22 µL, 0.29 mmol) was added and the reaction was allowed to stir over 24 hrs at ambient temperature. The reaction was diluted with water and extracted with EtOAc (30 mL). The organic layer was washed with water, brine, dried over $MgSO_4$, and concentrated under reduced pressure. The crude was purified through column chromatography leading to compound **26a** (0.04 g, 0.08 mmol) as an off white solid. ^{1}H NMR (400 MHz, $CDCl_3$) δ 7.18 (s, 1H), 7.12 (s, 1H), 6.99 (dd, *J* = 7.4, 6.0 Hz, 2H), 5.06 (s, 1H), 3.84 (t, J = 4.46 Hz, 4H), 3.58 (s, 3H), 2.68 (bt, 4H). ^{13}C NMR (101 MHz, $CDCl_3$) δ 167.13, 142.04, 132.69, 130.52, 130.16, 120.12, 118.85, 115.26, 115.03, 112.93, 66.81, 56.42, 42.05. HRMS [$C_{18}H_{17}N_3O_4F_3SCl_2^+$]: calcd 498.0269, found 498.0263.

2,4-Dichloro-5-((4-methylpiperazin-1-yl)sulfonyl)-N-(3,4,5-trifluorophenyl)-benzamide (28a). Compound **28a** was prepared from compound **27** (0.2 g, 0.57 mmol) and 3,4,5-trifuluro aniline following the synthetic technique for the preparation of **3a-3i**. Pure compound **28a** was obtained as white solid upon purification (silica gel, 10% MeOH/CH_2Cl_2). Yield = 65%. mp = 201.5^{O}C. ^{1}H NMR (400 MHz, DMSO-d_6) δ 11.04 (s, 1H), 8.14 (d, *J* = 6.4 Hz, 2H), 7.58 (dd, *J* = 9.9, 6.5 Hz, 2H), 3.24 (t, *J* = 4.49 Hz, 4H), 2.36 (t, J= 4.74 Hz, 4H), 2.18 (s, 3H). ^{13}C NMR (101 MHz, DMSO-d_6) δ 163.01, 135.55, 134.90, 134.72, 133.32, 133.09, 131.42, 104.42, 104.17, 53.91, 45.24. HRMS [$C_{18}H_{17}N_3O_3F_3SCl_2^+$]: calcd 482.0320, found 482.0340.

2,4-Dichloro-*N*-(3,5-dichloro-4-fluorophenyl)-5-((4-methylpiperazin-1-yl)sulfonyl)benzamide (28b). Compound **28b** was prepared from compound **27** (0.2g,

0.57 mmol) and 3,5-dichloro-4-fluro aniline following the synthetic technique for the preparation of **3a-3i**. Pure compound **28b** was obtained as white solid upon purification (silica gel, 10% MeOH/CH_2Cl_2). Yield = 64%. mp = 232.7 ^{O}C. ^{1}H NMR (400 MHz, DMSO) δ 11.00 (s, 1H), 8.15 (d, *J* = 14.8 Hz, 2H), 7.85 (d, *J* = 6.1 Hz, 2H), 3.23 (t, J = 4.38 Hz, 4H), 2.35 (t, J = 4.38 Hz, 4H), 2.18 (s, 3H). ^{13}C NMR (101 MHz, DMSO-d_6) δ 162.98, 135.57, 134.86, 134.73, 133.33, 133.10, 131.45, 121.10, 120.92, 120.20, 53.94, 45.41, 45.35. HRMS [$C_{18}H_{17}N_3O_3F_3SCl_2^+$]: calcd 513.9729, found = 513.9743.

2,4-Dichloro-*N*-(3,5-dichloro-4-fluorophenyl)-5-((4-methylpiperazin-1-yl)sulfonyl)-benzothioamide (29). Compound **29** was prepared from **28b** following the synthetic procedure for the preparation of **12**-**15**. Pure compound **29** was obtained as light purple solid upon purification (silica gel, 3% MeOH/CH_2Cl_2). Yield = 69%. ^{1}H NMR (400 MHz, $CDCl_3$) δ 9.60 (s, 1H), 8.04 (s, 1H), 7.94 (d, *J* = 5.8 Hz, 2H), 7.57 (s, 1H), 3.30 (bm, 4H), 2.47 (bm, 4H), 2.31 (s, 3H). ^{13}C NMR (101 MHz, DMSO) δ 141.62, 134.36, 133.63, 132.75, 131.74, 131.08, 123.93, 121.04, 120.85, 53.79, 45.18. HRMS [$C_{18}H_{17}N_3O_2FS_2Cl_4^+$]: calcd 529.9500, found = 529.9503.

Molecular modeling

The molecular modeling studies were performed using the induced fit docking protocol within the MOE software, as in prior studies.[2, 38] Briefly, hydrogen atoms and partial charges were added to crystal structure (PDB **3NKM**), and crystallographic water molecules were removed to produce the docking target.[22] Ligands were constructed in protonation and tautomeric states expected to predominate at pH 7.0. The docking target site was based on residues that fall within 5 Å of crystallographic LPA molecules found in crystal structures **3NKN**-**3NKR**.[22]

Testing of ATX inhibitors on ATX and LPAR

ATX Generation: Human recombinant ATX was expressed as published previously, using Sf9 *Spodoptera frugiperda* ovary cells (Invitrogen, Carlsbad, CA).[16] Suspension cells were grown to a 1 liter quantity at a concentration of $1x10^6$ cells/ml in Sf-900 III serum-free medium (Invitrogen) supplemented with 50 U/ml penicillin and 50 µg/ml streptomycin at 27°C with agitation. Cells were then infected with high-titer baculovirus generated via Bac-to-Bac Baculovirus Expression System (Invitrogen) using the pCMV5 mammalian expression vector containing the C-terminal FLAG-tagged human ATX sequence (a generous gift from Dr. Junken Aoki, Tohoku University, Sendai, Japan) subcloned into the pFastBac1 transfer vector. Expression was allowed to proceed for 72h, and secreted protein was harvested by centrifugation and filtration of the culture medium followed by affinity chromatography using anti-FLAG M2 agarose beads (Sigma-Aldrich, St. Louis, MO) and competitive elution with 50 µg/ml FLAG peptide (Sigma-Aldrich). Resultant ATX was then concentrated via centrifugation in Amicon Ultra 30,000 molecular weight cut off filter units (Millipore, Billerica, MA) and subsequent buffer exchange into storage buffer comprised of 50 mM Tris, pH 7.4 with 20% (v/v) ethylene glycol. Protein was held at -80°C for long-term storage.

ATX, ENPP6 and ENPP7 Inhibition: ATX activity was assessed via hydrolysis of the synthetic, lipid-like FRET-based substrate FS-3 (Echelon Biosciences, Salt Lake City, UT) or via hydrolysis of the nucleotide substrate p-nitrophenyl thymidine 5'-monophosphate (pNP-TMP) as described previously.[2] ENPP6 and ENPP7 activities were assessed by hydrolysis of the nucleotide substrate p-nitrophenylphosphorylcholine (pNPPC) as described previously.[13] Reaction wells were loaded in 60 µl volumes in

triplicate wells of half-area, black-wall 96-well plates in assay buffer consisting of 50 mM Tris, 140 mM NaCl, 5 mM KCl, 1 mM $CaCl_2$, 1 mM $MgCl_2$, 10 μM BSA, pH 8.0 for ATX; 100 mM Tris, 500 mM NaCl, 0.05% Triton, pH 9.0 for ENPP6; or 50 mM Tris, 150 mM NaCl, 10 mM taurocholate, pH 8.5 for ENPP7). For dose-response and IC_{50} generation, final concentrations per reaction well were comprised of 1 μM FS-3 (or 1 mM pNP-TMP), 0 or 4 nM human recombinant ATX and test compound concentrations ranging from 0 to 1 μM. For ENPP6 and ENPP7 screening, wells were comprised of 10 μM pNPPC, 0 or 10 nM ENPP6 or ENPP7 and a range of test compound concentrations of 0 to 10 μM. To determine mechanism of action, triplicate wells were loaded in assay buffer with FS-3 concentrations ranging from 0 to 10 μM, 0 or 4 nM ATX and inhibitor concentrations of 0, 0.5 x IC_{50} or 2 x IC_{50}. Fluorescence was read every 2 minutes for 1 hour at excitation/emission wavelengths of 485/528 nm for FS-3 hydrolysis or 405 nm absorbance for pNP-TMP of pNPPC hydrolysis using a FlexStation 3 microplate reader (Molecular Devices, Sunnyvale, CA). Data (relative fluorescence or absorbance) were then recorded as a mean value of the triplicates for each sample versus time. Percent ATX, ENPP6 or ENPP7 activity (±SD) were calculated from the 1 hour time point data for each inhibitor concentration, and GraphPad Prism version 5.0a (GraphPad Software, San Diego, CA) was then used to fit non-linear regression curves, fitting the Hill Slope from the data in a variable slope model and interpolating from the curve to determine the IC_{50} (±SD) for each compound. In the case of mechanism determination, the linear fluorescence data from time 10 minutes to 30 minutes were then transformed using a carboxyfluorescein standard curve to determine product concentration and plotted separately. Linear trend lines were inserted using Microsoft Excel, the slope of which

represent the rates of reaction for each substrate concentration. This reaction rate data for each inhibitor concentration were then plotted against substrate (FS-3) concentration and simultaneously fitted via non-linear regression in the Michaelis-Menten equations for competitive, non-competitive, uncompetitive, and mixed-mode inhibition using GraphPad Prism version 5.0a. Mechanism of inhibition was determined by which curve fit had the best global fit (R^2 value).

Selective dose dependent inhibition of LPA1 receptor by 3b, 3f, and 3g.

Cell Culture: LPA1 and LPA3 RH7777 rat hepatoma cells were generated in-house as described previously[39] and maintained in DMEM supplemented with 10% FBS and 2 mM L-glutamine with 250 µg/ml G418. LPA2 MEF mouse embryonic fibroblast cells were also derived from LPA1 and LPA2 double knockout mouse embryos as described previously[40] and maintained in DMEM supplemented with 10% FBS, 2 mM L-glutamine, 100 U/ml penicillin and 100 µg/ml streptomycin. LPA_4 CHO chinese hamster ovary cells were a generous gift from Dr. Takao Shimizu (Tokyo University, Tokyo, Japan) and were maintained in Ham's F12 medium supplemented with 10% FBS, 2 mM L-glutamine and 350 µg/ml G418. LPA5 B103 rate neuroblastoma cells were derived in house via lentiviral transduction of FLAG-tagged LPA5 and puromycin selection as published[41] and maintained in DMEM supplemented with 10% FBS and 0.4 µg/ml puromycin. All cells were maintained at 37°C with 5% CO_2 in a humidified atmosphere.

Calcium Mobilization Assay: As published previously, LPAR activation leads to transient calcium mobilization. In order to assess receptor activation or antagonism, compounds were tested in stable transfectant cell lines engineered to overexpress a single LPAR subtype.[35] At the level of each receptor, calcium mobilization was assessed via

fluorescence in Fura-2AM-loaded cells treated with a dose range of test compound both in the absence and presence of the EC_{50} concentration of LPA 18:1 corresponding to the appropriate receptor subtype and cell line. All cells were plated in triplicate in 96-well, black-wall plates at a density of $5x10^4$ cells per well and allowed to adhere overnight. LPA1 and LPA3 RH7777 cells were plated in poly-L-lysine coated plates. LPA5 B103 cells were plated in Matrigel-coated plates. After adherence, cells were serum-deprived in Krebs buffer consisting of 10 mM HEPES, pH 7.4 with 120 mM NaCl; 5 mM KCl; 1.8 mM $CaCl_2$; 0.62 mM $MgSO_4$; 6 mM D-glucose. LPA1 RH7777, LPA3 RH7777 and LPA5 B103 cells were serum-deprived for 4 hours, while LPA2 MEF cells were serum-deprived for 1 hour, and LPA4 CHO cells were not serum-deprived. Fura 2-AM was then loaded for 30 minutes at a concentration of 4.5 μg/ml in Krebs buffer with 0.45% (v/v) Pluronic F-127 (and additionally 0.1% BSA and 2.5 mM Probenicid for LPA4 CHO cells), after which cells were switched to fresh Krebs buffer. Finally, the robotics of a FlexStation 3 microplate reader were used to apply a dose-range of LPA 18:1 (in a 1:1 molecular complex with lipid-depleted BSA) or test compounds ranging from 0 to 100 μM in the presence and absence of the EC_{50} concentration of LPA 18:1 for each LPA receptor subtype. Fluorescence corresponding to calcium mobilization was immediately monitored upon addition every 3.42 seconds over a span of 70 seconds total at excitation/emission wavelengths of 340/510 and 380/510 nm. Data (relative fluorescence) were then recorded as a mean fluorescence ratio value of the triplicates for each concentration and normalized to percentage of LPA 18:1 E_{max}. GraphPad Prism version 5.0a was then used to plot the data and fit non-linear

regression curves in a variable slope model in order to determine the pharmacodynamics (EC_{50} or IC_{50}) of the compounds in Ca^{2+} mobilization.

In vitro invasion assay - A2058 human melanoma cell line (gift from Dr. Timothy Clair, NCI, National Institutes of Health) was cultured in Dulbecco's modified Eagle's medium (DMEM) supplemented with 10% (V/V) FBS, 100 U/mL penicillin, 100 µg/mL streptomycin and 2mM L-glutamine (Life Technologies). Cell invasion was performed using the 24-well BD Biocoat^{TM} tumor invasion system (BD Biosciences, 8µm-pore size). Briefly, the matrigel coating was rehydrated with PBS at 37°C for 2 h. After removal of PBS, 5 x 10^4 A2058 cells in serum-free DMEM supplemented with 0.1% BSA were plated to each upper chamber. 0.75 ml of serum-free DMEM/0.1% BSA containing chemoattractant (recombinant ATX plus 1µM of 18:1 LPC) with or without the respective ATX inhibitors was added to the bottom chamber. Cells were allowed to invade the matrigel for 20 h at 37°C. To stain the invaded cells, the media in the upper chamber was first removed and the insert was transferred to a new 24-well plate containing 4µg/ml of Calcein AM (Molecular Probes, Life Technologies) in Hank's balanced salt solution (HBSS) and incubated for 1 h at 37°C. The fluorescent invaded cells were measured using the FLEXstation II plate reader (Molecular Devices) at excitation and emission wavelengths of 485 and 530nm, respectively.

Cell growth assay for cytotoxicity and chemoresistance of 4T1 cells. – To assess cytotoxicity of benzene sulfonamide ATX inhibitors, wild-type 4T1 cells were plated in 96-well plates at a density of 7,500 cells per well in RPMI with 1% (v/v) charcoal-stripped FBS and incubated 4h at 37°C with 5% CO_2. Cells were then treated for 48h with 0 – 10 µM benzene sulfonamide ATX inhibitors or the reference ATX inhibitor **30**

with daily refreshment of compound treatment. Viability was assessed via Promega CellTiter Blue reagent as per manufacturer's instructions and subsequently normalized to % vehicle control. For chemoresistance studies, wild-type 4T1 cells were plated in 96-well plates at a density of 5,000 cells per well in RPMI with 1% (v/v) charcoal-stripped FBS and incubated overnight at 37°C with 5% CO_2. Cells were then treated for 24 h with 3 μM ATX or ATX/LPA1 inhibitors followed by 48h treatment with a dose range of 0 – 1 μM PT in RPMI with 1% (v/v) charcoal-stripped FBS. After 48h incubation, cells were allowed to recover in RPMI with 10% FBS for an additional 72h. Viability was then assessed via Promega CellTiter Blue following manufacturer's instructions and normalized to % vehicle control samples. All viability data were plotted using GraphPad Prism, and non-linear regression analysis was performed in a variable slope model in order to determine LD_{50} concentrations for ATX inhibitors alone or PT in the presence and absence of ATX inhibitors. The 4T1-TaxR cell line was generated by treating wild-type 4T1 at increasing doses of PT from 40nM, 100nM to 200nM. Briefly, 1.5 x 10^5 cells per 10cm dish were treated at each PT dose for 7 days with daily replenishment and allowed to recover for 7 days before the start of the next increment dose of PT treatment. To generate mammospheres, 3.5 x 10^3 4T1-TaxR cells were plated in each well of a 24-well plate in serum free RPMI supplemented with 1x N2 supplement, 20ng/mL of FGF and 20ng/mL of EGF. Cells were cultured at 37°C with 5% CO_2 for 4 days to allow sphere formation. At day 4, spheres were treated with or without PT 100nM and the various ATX inhibitors at 5μM as indicated for 3 days. Viability was then assessed using the Promega CellTiter Blue reagent.

***In vivo* lung metastasis study**. All animal procedures were approved by the Institutional Animal Care and Use Committee (IACUC) at the University of Tennessee Health Science Center. B16F10 murine melanoma cells were cultured in Minimum Essential Medium (MEM) supplemented with 5% (V/V) heat-inactivated FBS, 2mM L-glutamine (Life Technologies), 1% (V/V) MEM-vitamin solution, 1mM sodium pyruvate and 1% (V/V) non-essential amino acids (NEAA). Briefly, 1 x 10^5 cells were injected into the tail vein of 8 to 12 week old C57BL/6 mice purchased from Jackson Laboratory (Bar Harbor, ME). Mice were treated either with vehicle (PBS containing 1% DMSO and 50μM charcoal-stripped mouse serum albumin (MSA)) or the ATX inhibitors as indicated. Treatment began at day 0 (prior to tumor inoculation) via intraperitoneal injection of 1 mg/kg of compound and continued daily for up to day 10. All mice were sacrificed at day 21. The number of metastatic tumor nodules on the lungs was counted.

***In vitro* stability determination by LC-MS.** To assess stability of amide (and thioamide) analogs in short term *in vitro* assays, 4T1 mouse mammary carcinoma cells (1 x 104 cells per well) were plated in 48-well plates (a concentration equivalent to that used in the cytotoxicity/viability assay described). The cells were allowed to attach and recover overnight before 550 μL of fresh DMEM containing 1% charcoal stripped FBS and 10 μM of either **3**, **3b**, **3f**, or **14** was added (with a final concentration of 0.1% DMSO). Quadruplicate samples were taken at time 0, 16 and 40h post treatment for analysis by LC-MS/MS. All samples were centrifuged at 16,000 x g for 3 min at 4°C to remove cell debris and 500 μL aliquots were extracted twice with 500 μL of diethyl ether. The pooled organic extracts were dried under N2 before analysis by LC-MS/MS

(for the amide analogs **3**, **3b**, and **3f**) or LC-MS for the thioamide analog **14**) using a Thermo LTQ-XL mass spectrometer. Target compounds were isolated using a C18 column with a solvent gradient starting with 60% solvent A for 1 min with a linear gradient to 100% solvent B by 4 min. This composition was maintained for an additional 2 min before returning to 100% solvent A for a total run time of 8 min (solvent A: water + 0.025% NH4OH, solvent B: methanol + 0.025% NH4OH). The following parent to product ion MS/MS transitions were monitored for **3** (430.9 to 293.4 m/z), **3b** (469.9 to 430.8 m/z), and **3f** (484.8 to 448.8 m/z). Since MS/MS of **14** resulted in very low signals, this compound was analyzed following its parent ion at 482.7 m/z. Peak areas for each MS/MS transitions (or parent ion) were determined and normalized to the 0h control.

Supporting Information

^{1}H NMR, ^{13}C NMR for target compounds.

Molecular formula strings.

PDB ID Codes: **3** (PDB 3NKM) and **3b (**PDB 3NKM**)**. Authors will release the atomic coordinates an experimental data upon article publication.

Corresponding Authors

Duane D. Miller, Ph.D. Email. dmiller@uthsc.edu. Phone. (+1)-901-448-6026. Gabor J. Tigyi, Ph.D., M.D. Email. gtigyi@uthsc.edu. Phone. (+1)-901-448-2634.

Acknowledgement.

This work is supported by NIH/NCI grants CA-092160 to Dr. Gabor G. Tigyi and Dr. Duane D. Miller. Its contents are solely the responsibility of the authors and do not necessarily represent the official views of the NIH/NCI.

Abbreviations Used

ATX, autotaxin; LPA, lysophosphatidic acid ; LPC, lysophosphatidylcholine ; LPAR, lysophosphatidic acid receptor; GPCR, G protein-coupled receptor; ENPP, ecto nucleotide phosphodiesterase; pNPPC, p-nitrophenylphophorylcholine ; IC_{50}, half maximum inhibitory concentration; SAR, structure-activity relationship; MOE, molecular operating environment; pNP-TMP, p-nitrophenyl thymidylate; DMEM, Dulbecco's modified Eagle's medium ; HBSS, Hank's balanced salt solution ; IACUC, Institutional Animal Care and Use Committee ; NEAA, non-essential amino acids ; MSA, mouse serum albumin

References

1. Castagna, D.; Budd, D. C.; Macdonald, S. J.; Jamieson, C.; Watson, A. J. Development of autotaxin inhibitors: an overview of the patent and primary literature. *J. Med. Chem.* **2016,** *59*, 5604-5621

2. Fells, J. I.; Lee, S. C.; Norman, D. D.; Tsukahara, R.; Kirby, J. R.; Nelson, S.; Seibel, W.; Papoian, R.; Patil, R.; Miller, D. D.; Parrill, A. L.; Pham, T. C.; Baker, D. L.; Bittman, R.; Tigyi, G. Targeting the hydrophobic pocket of autotaxin with virtual

screening of inhibitors identifies a common aromatic sulfonamide structural motif. *FEBS J.* **2014,** *281*, 1017-1028

3. Albers, H. M.; Ovaa, H. Chemical evolution of autotaxin inhibitors. *Chem. Rev.* **2012,** *112*, 2593-2603

4. Kihara, Y.; Mizuno, H.; Chun, J. Lysophospholipid receptors in drug discovery. *Exp. Cell Res.* **2015,** *333*, 171-177

5. Tigyi, G. Aiming drug discovery at lysophosphatidic acid targets. *Br. J. Pharmacol.* **2010,** *161*, 241-270

6. Brindley, D. N.; Lin, F. T.; Tigyi, G. J. Role of the autotaxin-lysophosphatidate axis in cancer resistance to chemotherapy and radiotherapy. *Biochim. Biophys. Acta.* **2013,** *1831*, 74-85

7. Baker, D. L.; Fujiwara, Y.; Pigg, K. R.; Tsukahara, R.; Kobayashi, S.; Murofushi, H.; Uchiyama, A.; Murakami-Murofushi, K.; Koh, E.; Bandle, R. W.; Byun, H. S.; Bittman, R.; Fan, D.; Murph, M.; Mills, G. B.; Tigyi, G. Carba analogs of cyclic phosphatidic acid are selective inhibitors of autotaxin and cancer cell invasion and metastasis. *J. Biol. Chem.* **2006,** *281*, 22786-22793

8. Sue-Chin., L.; Yuko., F.; ., L. J.; Junming., Y.; Yaohong., W.; Ryoko., T.; Erzsebet., S.; Renukadevi., P.; Souvik., B.; Duane., M. D.; ., B. L.; ., G. C. M.; Christopher., W. M.; Tamas., O.; Tigyi, G. J. Autotaxin, lysophosphatidic acid receptors 1 and 5 exert different functions in tumor cells versus the host tissue microenvironment in melanoma invasion and metastasis. *Mol. Cancer Res.* **2015,** *13*, 174-185

9. Seo, E. J.; Kwon, Y. W.; Jang, I. H.; Kim, D. K.; Lee, S. I.; Choi, E. J.; Kim, K. H.; Suh, D. S.; Lee, J. H.; Choi, K. U.; Lee, J. W.; Mok, H. J.; Kim, K. P.; Matsumoto, H.;

Aoki, J.; Kim, J. H. Autotaxin regulates maintenance of ovarian cancer stem cells through lysophosphatidic acid-mediated autocrine mechanism. *Stem Cells* **2016,** *34*, 551-564

10. Albers, H. M.; Hendrickx, L. J.; van Tol, R. J.; Hausmann, J.; Perrakis, A.; Ovaa, H. Structure-based design of novel boronic acid-based inhibitors of autotaxin. *J. Med. Chem.* **2011,** *54*, 4619-4626

11. Albers, H. M.; van Meeteren, L. A.; Egan, D. A.; van Tilburg, E. W.; Moolenaar, W. H.; Ovaa, H. Discovery and optimization of boronic acid based inhibitors of autotaxin. *J. Med. Chem.* **2010,** *53*, 4958-4967

12. Castagna, D.; Duffy, E. L.; Semaan, D.; Young, L. C.; Pritchard, J. M.; Macdonald, S. J. F.; Budd, D. C.; Jamieson, C.; Watson, A. J. B. Identification of a novel class of autotaxin inhibitors through cross-screening. *Med. Chem. Commun.* **2015,** *6*, 1149-1155

13. Gupte, R.; Patil, R.; Liu, J.; Wang, Y.; Lee, S. C.; Fujiwara, Y.; Fells, J.; Bolen, A. L.; Emmons-Thompson, K.; Yates, C. R.; Siddam, A.; Panupinthu, N.; Pham, T. C.; Baker, D. L.; Parrill, A. L.; Mills, G. B.; Tigyi, G.; Miller, D. D. Benzyl and naphthalene methylphosphonic acid inhibitors of autotaxin with anti-invasive and anti-metastatic activity. *ChemMedChem* **2011,** *6*, 922-935

14. Hoeglund, A. B.; Bostic, H. E.; Howard, A. L.; Wanjala, I. W.; Best, M. D.; Baker, D. L.; Parrill, A. L. Optimization of a pipemidic acid autotaxin inhibitor. *J. Med. Chem.* **2010,** *53*, 1056-1066

15. Stein, A. J.; Bain, G.; Prodanovich, P.; Santini, A. M.; Darlington, J.; Stelzer, N. M.; Sidhu, R. S.; Schaub, J.; Goulet, L.; Lonergan, D.; Calderon, I.; Evans, J. F.;

Hutchinson, J. H. Structural basis for inhibition of human autotaxin by four potent compounds with distinct modes of binding. *Mol. Pharmacol.* **2015,** *88*, 982-992

16. Fells, J. I.; Lee, S. C.; Fujiwara, Y.; Norman, D. D.; Lim, K. G.; Tsukahara, R.; Liu, J.; Patil, R.; Miller, D. D.; Kirby, R. J.; Nelson, S.; Seibel, W.; Papoian, R.; Parrill, A. L.; Baker, D. L.; Bittman, R.; Tigyi, G. Hits of a high-throughput screen identify the hydrophobic pocket of autotaxin/lysophospholipase D as an inhibitory surface. *Mol. Pharmacol.* **2013,** *84*, 415-424

17. Mize, C. D.; Abbott, A. M.; Gacasan, S. B.; Parrill, A. L.; Baker, D. L. Ligand-based autotaxin pharmacophore models reflect structure-based docking results. *J. Mol. Graph. Model.* **2011,** *31*, 76-86

18. Barbayianni, E.; Magrioti, V.; Moutevelis-Minakakis, P.; Kokotos, G. Autotaxin inhibitors: a patent review. *Expert Opin. Ther. Pat.* **2013,** *23*, 1123-1132

19. Katsamakas, S.; Bermperoglou, E.; Hadjipavlou-Litina, D. Considering autotaxin inhibitors in terms of 2D-QSAR and 3D-mapping- review and evaluation. *Curr. Med. Chem.* **2015,** *22*, 1428-1461

20. Saga, H.; Ohhata, A.; Hayashi, A.; Katoh, M.; Maeda, T.; Mizuno, H.; Takada, Y.; Komichi, Y.; Ota, H.; Matsumura, N.; Shibaya, M.; Sugiyama, T.; Nakade, S.; Kishikawa, K. A novel highly potent autotaxin/ENPP2 inhibitor produces prolonged decreases in plasma lysophosphatidic acid formation in vivo and regulates urethral tension. *PLoS One* **2014,** *9*, e93230

21. Hausmann, J.; Kamtekar, S.; Christodoulou, E.; Day, J. E.; Wu, T.; Fulkerson, Z.; Albers, H. M.; van Meeteren, L. A.; Houben, A. J.; van Zeijl, L.; Jansen, S.; Andries, M.; Hall, T.; Pegg, L. E.; Benson, T. E.; Kasiem, M.; Harlos, K.; Kooi, C. W.; Smyth, S. S.;

Ovaa, H.; Bollen, M.; Morris, A. J.; Moolenaar, W. H.; Perrakis, A. Structural basis of substrate discrimination and integrin binding by autotaxin. *Nat. Struct. Mol. Biol.* **2011,** *18*, 198-204

22. Nishimasu, H.; Okudaira, S.; Hama, K.; Mihara, E.; Dohmae, N.; Inoue, A.; Ishitani, R.; Takagi, J.; Aoki, J.; Nureki, O. Crystal structure of autotaxin and insight into GPCR activation by lipid mediators. *Nat. Struct. Mol. Biol.* **2011,** *18*, 205-U271

23. Gierse, J.; Thorarensen, A.; Beltey, K.; Bradshaw-Pierce, E.; Cortes-Burgos, L.; Hall, T.; Johnston, A.; Murphy, M.; Nemirovskiy, O.; Ogawa, S.; Pegg, L.; Pelc, M.; Prinsen, M.; Schnute, M.; Wendling, J.; Wene, S.; Weinberg, R.; Wittwer, A.; Zweifel, B.; Masferrer, J. A novel autotaxin inhibitor reduces lysophosphatidic acid levels in plasma and the site of inflammation. *J. Pharmacol. Exp. Ther.* **2010,** *334*, 310-317

24. Furminger, V.; Hughes, O. R.; Legrand, D. M.; Stanley, E.; Thomson, C. Preparation of N-substituted nonaryl-heterocyclo carboxylate as autotaxin inhibitors. U.S. Pat. Appl. 2014/0171404 A1, 2014

25. Kato, K.; Ikeda, H.; Miyakawa, S.; Futakawa, S.; Nonaka, Y.; Fujiwara, M.; Okudaira, S.; Kano, K.; Aoki, J.; Morita, J.; Ishitani, R.; Nishimasu, H.; Nakamura, Y.; Nureki, O. Structural basis for specific inhibition of autotaxin by a DNA aptamer. *Nat. Struct. Mol. Biol.* **2016,** *23*, 395-401

26. Banerjee, S.; Smith, J.; Smith, J.; Faulkner, C.; Masterson, D. S. A stereoselective cyclization strategy for the preparation of gamma-lactams and their use in the synthesis of alpha-methyl-beta-proline. *J. Org. Chem.* **2012,** *77*, 10925-10930

27. Pelcman, B.; Olofsson, K.; Suna, E.; Kalvins, I.; Ozola, V.; Andrianov, V. Disulfonamides useful in the treatment of inflammation. Int. Pat. Appl. WO2008129276 A1, 2008

28. Rashad, A. A.; Jones, A. J.; Avery, V. M.; Baell, J.; Keller, P. A. Facile synthesis and preliminary structure-activity analysis of new sulfonamides against trypanosoma brucei. *ACS Med. Chem. Lett.* **2014,** *5*, 496-500

29. Cholody, W. M.; Zang, Y.; Zuck, K.; Watthey, J. W. H.; Ohler, Z.; Strovel, J.; Ohler, N. E.; Chellappan, S.; Padia, J. Derivatives of multi-ring aromatic compounds and uses as anti-tumor agents. Int. Pat. Appl. WO 2010082912 A1, 2010

30. Alyar, S.; Özbek, N.; Kuzukıran, K.; Karacan, N. Quantitative structure–activity relationships studies for prediction of antimicrobial activity of synthesized disulfonamide derivatives. *Med. Chem. Res.* **2010,** *20*, 175-183

31. Cacchi, S.; Fabrizi, G.; Goggiamani, A.; Licandro, E.; Maiorana, S.; Perdicchia, D. Synthesis of N,N-Dialkyl-N'-arylhydrazines via palladium-catalyzed N-arylation by using N,N-dialkylhydrazines/2LiCl adducts. *Org. Lett.* **2005,** *7*, 1497-1500

32. De Luca, L.; Giacomelli, G. An easy microwave-assisted synthesis of sulfonamides directly from sulfonic acids. *J. Org. Chem.* **2008,** *73*, 3967-3969

33. Kim, J. G.; Jang, D. O. Mild and efficient indium metal catalyzed synthesis of sulfonamides and sulfonic esters. *Synlett* **2007,** *2007*, 2501-2504

34. Rosen, B. R.; Ruble, J. C.; Beauchamp, T. J.; Navarro, A. Mild Pd-catalyzed N-arylation of methanesulfonamide and related nucleophiles: avoiding potentially genotoxic reagents and byproducts. *Org. Lett.* **2011,** *13*, 2564-2567

35. Zhang, H.; Xu, X.; Gajewiak, J.; Tsukahara, R.; Fujiwara, Y.; Liu, J.; Fells, J. I.; Perygin, D.; Parrill, A. L.; Tigyi, G.; Prestwich, G. D. Dual activity lysophosphatidic acid receptor pan-antagonist/autotaxin inhibitor reduces breast cancer cell migration in vitro and causes tumor regression in vivo. *Cancer Res.* **2009,** *69*, 5441-5449

36. Venkatraman, G.; Benesch, M. G.; Tang, X.; Dewald, J.; McMullen, T. P.; Brindley, D. N. Lysophosphatidate signaling stabilizes Nrf2 and increases the expression of genes involved in drug resistance and oxidative stress responses: implications for cancer treatment. *FASEB J.* **2015,** *29*, 772-785

37. Hrast, M.; Turk, S.; Sosic, I.; Knez, D.; Randall, C. P.; Barreteau, H.; Contreras-Martel, C.; Dessen, A.; O'Neill, A. J.; Mengin-Lecreulx, D.; Blanot, D.; Gobec, S. Structure-activity relationships of new cyanothiophene inhibitors of the essential peptidoglycan biosynthesis enzyme MurF. *Eur. J. Med. Chem.* **2013,** *66*, 32-45

38. Norman, D. D.; Ibezim, A.; Scott, W. E.; White, S.; Parrill, A. L.; Baker, D. L. Autotaxin inhibition: development and application of computational tools to identify site-selective lead compounds. *Bioorg. Med. Chem.* **2013,** *21*, 5548-5560

39. Halgren, T. A. MMFF VI. MMFF94s option for energy minimization studies. *J. Comput. Chem.* **1999,** *20*, 720-729

TABLES:

Table 1. Structure-activity relationship of the new ATX inhibitors

Compounds	IC_{50} (nM ± SD) vs FS-3	pNP-TMP Inhibition	Mechanism	Log P	Molecular Weight
3	117 ± 2	None	Competitive	2.99	433.28
3a	32 ± 2	None	Competitive	3.17	451.27
3b	9 ± 0.2	None	Competitive	3.23	469.26
3c	1,034 ± 120	None	ND	3.67	505.24
3d	> 1,000	None	ND	4.35	518.63
3e	> 1,000	None	ND	2.91	505.36
3f	84 ± 0.1	None	Competitive	3.62	485.72
3g	40 ± 0.3	None	Competitive	3.89	502.17
3h	190 ± 13	None	ND	2.46	476.28
3i	864 ± 52	None	ND	2.78	509.31

4	> 1,000	None	ND	2.26	476.83
5	18 ± 2	None	ND	3.71	548.16
7	> 1000	None	ND	2.74	431.26
8	> 1000	None	ND	3.42	448.27
9	> 1000	None	ND	2.56	447.31
10	> 1000	None	ND	3.92	437.29
11	396 ± 44	None	ND	3.98	455.28
12	121 ± 1	None	ND	3.57	449.35
13	70 ± 1	None	ND	3.72	467.34
14	35 ± 3	None	Competitive	3.87	485.33
15	98 ± 7	None	ND	4.95	518.24
19	> 1,000	None	ND	1.92	469.33
20	> 1,000	None	ND	2.65	627.48
22	> 1,000	None	ND	1.91	469.33
23	> 1,000	None	ND	2.06	505.32
25	> 1,000	None	ND	3.49	420.21
26a	> 1,000	None	ND	2.83	498.30
28a	67 ± 7.1	None	ND	3.23	482.30
28b	56 ± 9	None	ND	3.53	515.21
29	100 ± 8	None	ND	4.38	531.28

Footnotes: Note. ND = not determined. Log P was calculated using Schrödinger Molecular Modeling Suite®. Schrödinger LLC. New York.

Table 2. Effect of ATX inhibitors on LPA-mediated Ca^{2+} mobilization

Note. NE = no effect detected.

	LPA_1		**LPA_2**		**LPA_3**		**LPA_4**		**LPA_5**	
	EC_{50} or IC_{50} (μM)	E_{max}	EC_{50} or IC_{50} (μM)	E_{max}	EC_{50} or IC_{50} (μM)	E_{max}	EC_{50} or IC_{50} (μM)	E_{max}	EC_{50} or IC_{50} (μM)	E_{max}
LPA1 18:1	0.08 ± 0.01	100.0 0 ± 0.00	0.003 ± 0.00	100.0 0 ± 0.00	0.29 ± 0.01	100.0 0 ± 0.00	0.57 ± 0.01	100.0 0 ± 0.00	0.14 ± 0.00	100.0 0 ± 0.00
LPA + **3b**	14.47 ± 2.75	46.14 ± 15.54	NE	NE	NE	NE	NE	NE	NE	NE

LPA + **3f**	6.12 ± 2.22	51.03 ± 13.99	NE	NE	NE	NE	NE	NE	NE	NE
LPA + **3g**	18.39 ± 7.44	50.04 ± 13.04	NE	NE	NE	NE	NE	NE	NE	NE
LPA + **14**	NE	NE	NE	NE	NE	NE	NE	NE	NE	NE
LPA + **5**	NE	NE	NE	NE	NE	NE	NE	NE	NE	NE

Table 3. IC_{50} values of compounds **3b**, **3a**, and **14** in the A2058 cell invasion assay

Compounds	IC_{50} (nM)
3b	528 ± 14
3a	1478 ± 12
3f	740.4 ± 13
14	403 ± 13

Figure Legends

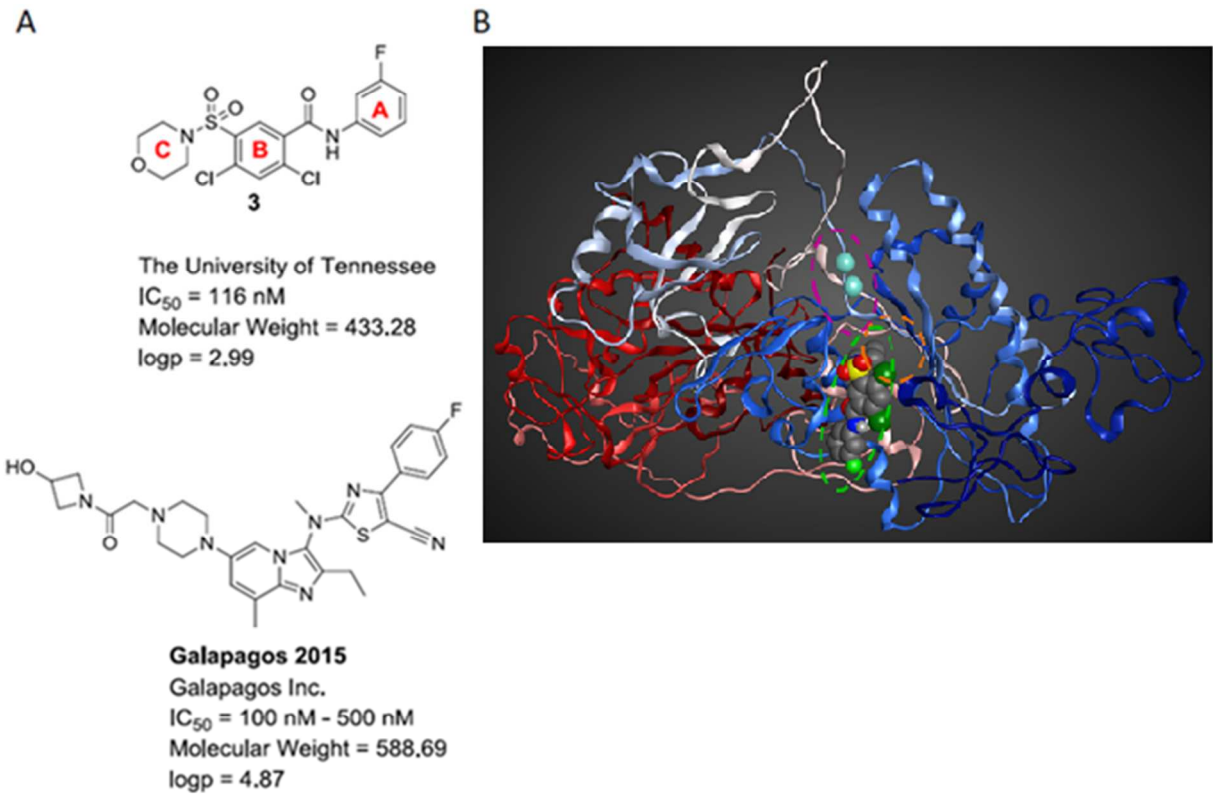

Figure 1. Panel A. Examples of non-acidic head group non-lipid ATX inhibitors.[1, 2, 3] **Galapagos 2015** is one of the non-carboxylic acid autotaxin inhibitors developed and reported by Galapagos Inc. in 2015.[3] Panel B. Position of top-ranked pose of **3** (Space-filling model) in the mouse ATX crystal structure (PDB **3NKM**) represented as a ribbon shaded from blue at the amino-terminus to red at the carboxy-terminus. Position of **3** is outside of the catalytic core of the ATX active site (enclosed in dotted magenta circle). Catalytic site metal ions are shown as cyan spheres. The additional outlined areas are the hydrophobic pocket (orange) and the hydrophobic tunnel (green).

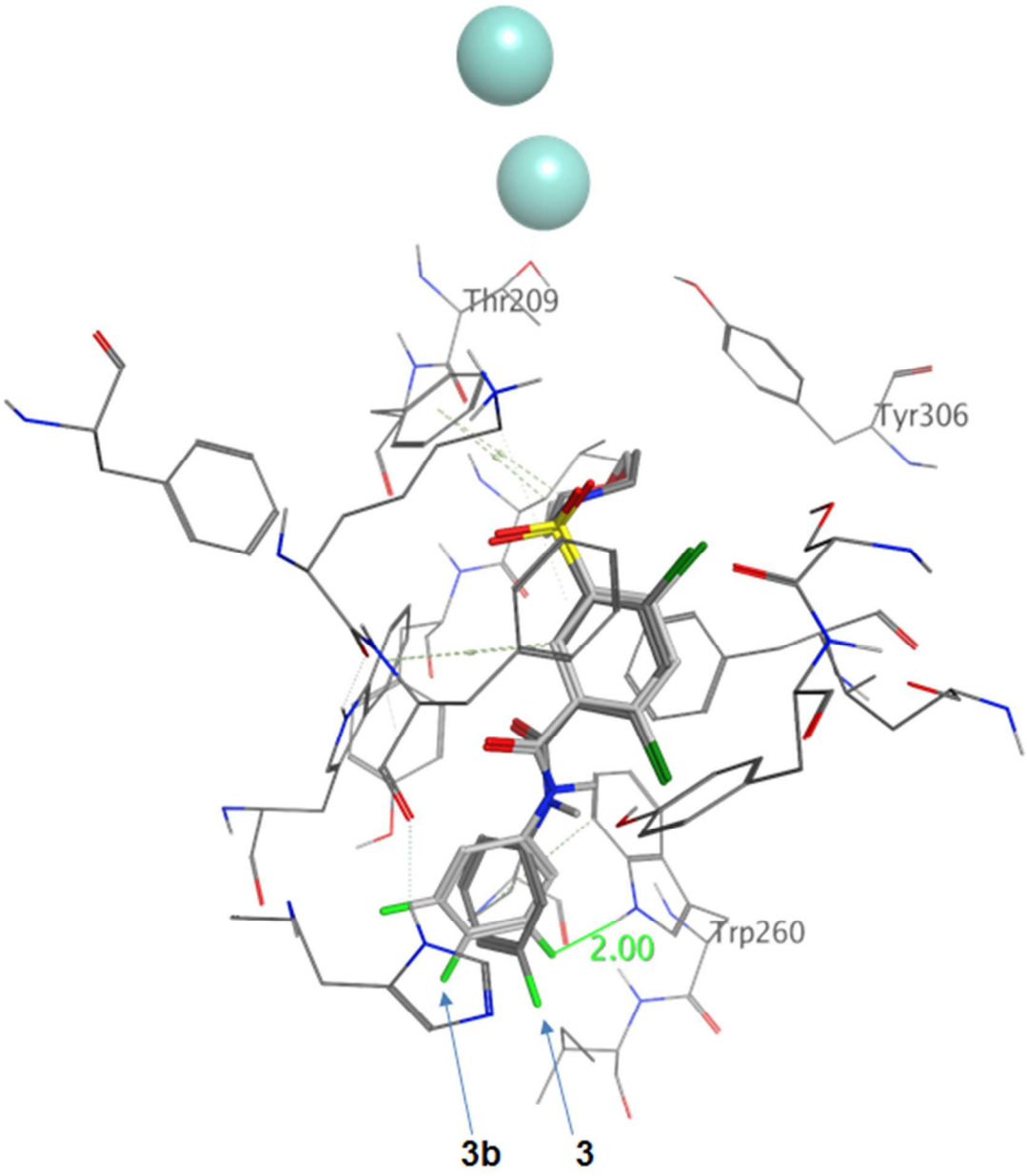

Figure 2. . Binding poses (low energy conformation) of **3** (dark grey carbon atoms) and **3b** (light grey carbon atoms) in ATX crystal structure (PDB **3NKM**). Distance measured between a fluorine atom of **3b** and the aromatic amine hydrogen of W260 in ATX is shown in green.

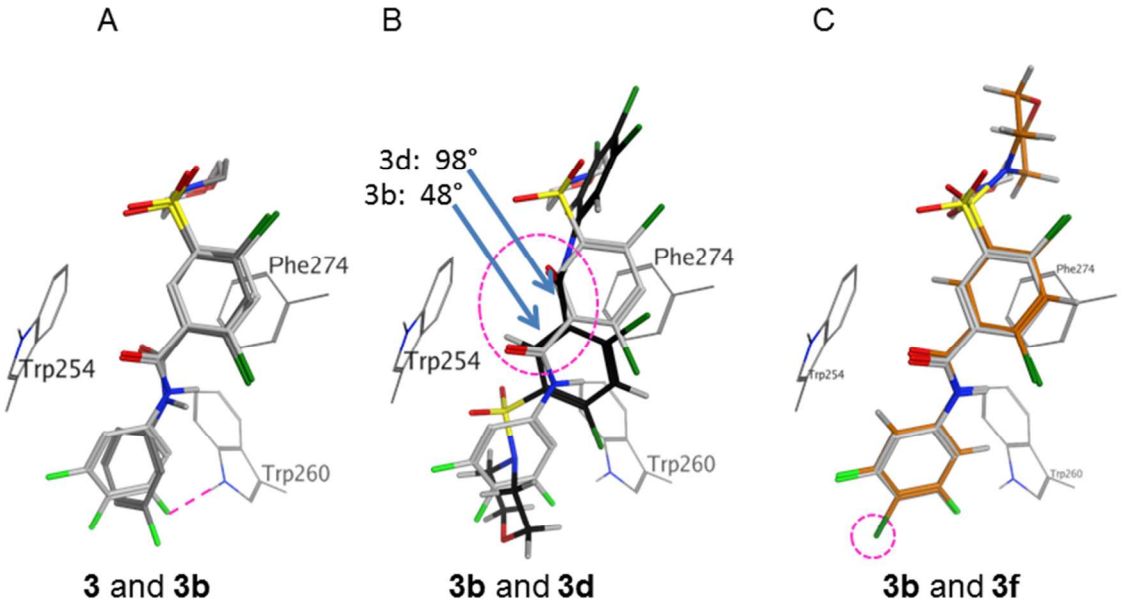

Figure 3. Molecular models of ATX inhibitors docked into ATX crystal structure (PDB **3NKM**). Superpositions of compound **3b** (light grey carbons) with **3** (dark grey carbons) (panel A), **3d** (black carbons) (panel B), and **3f** (orange carbons) (panel C) explain observed potency differences. Panel A displays the hydrogen bond formed between the 3-fluoro group of tri-fluorinated compound **3b** (magenta dotted line) that the 3-fluoro group of the less electron-rich mono-fluorinated compound **3** does not form. The additional hydrogen bond formed by **3b** is consistent with the more potent inhibition of ATX observed for **3b** relative to the parent compound. Panel B illustrates the inability of trichlorinated compound **3d** to adopt a pose similar to that seen for trifluorinated compound **3b**. The larger size of the three chlorine substituents of **3d** is not accommodated within the hydrophobic tunnel at the lower left corner, and the best-ranked pose has a poorly-conjugated linkage between the central aryl group and the amide linker in the region encircled in the magenta dotted line (98° torsion angle relative

to preferred angle in isolation of 40°). The pose of **3b** exhibits much lower conformational distortion with a 48° torsion angle for the corresponding bond. The difference in energy between the docked conformation of **3d** and the closest local minimum energy (both in the absence of the protein and computed using the MMFF94 forcefield)[39] is over 15 kcal/mol. The difference for **3b** is less than 3 kcal/mol. Thus **3d** has a 12 kcal/mol greater conformational energy penalty than **3b**. Panel C shows excellent superposition of the trihalogenated aromatic rings of **3b** and **3f**, with the 4-halo substituent exposed to the aqueous solution that would fill the remainder of the hydrophobic tunnel. The larger and less electronegative chlorine atom has sufficient space in the 4-position to allow adoption of a similar binding pose, but lowers potency due to lower preference for aqueous exposure relative to the 4-fluoro substituent of **3b**.

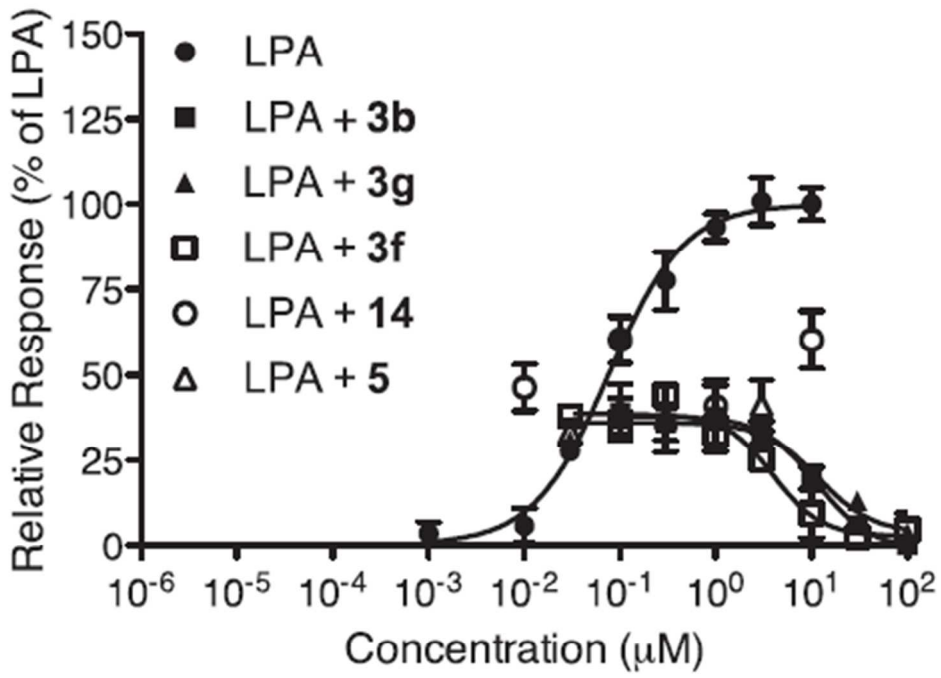

Figure 4. Effect of ATX inhibitors on LPA-activated Ca^{2+} responses mediated by LPA_1 RH7777 cells. All measurements were done in quadruplicates and data represent the mean ± SD.

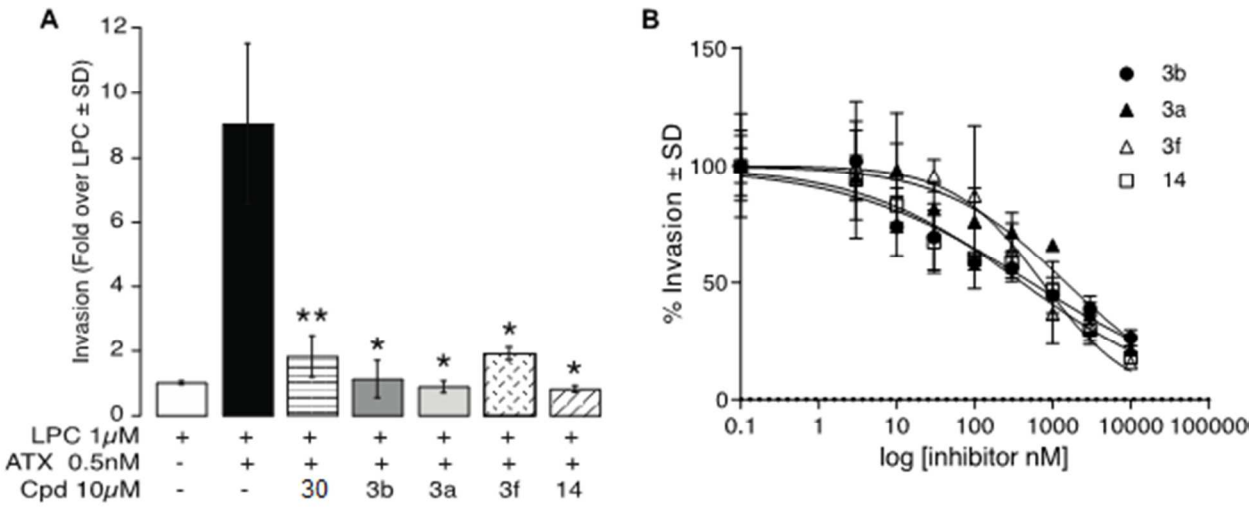

Figure 5 Characterization of ATX inhibitors on A2058 human melanoma invasion. (Panel A) Effect of the various ATX inhibitors on A2058 cell invasion. (Panel B) Dose response curves were generated in the presence of exogenous LPC, recombinant ATX and increasing concentrations of inhibitors as indicated. All measurements were done in triplicates and data represent the mean ± SD of an experiment performed three times. **p<0.001 and *p<0.0001 relative to LPC plus ATX treatment based on 1-way ANOVA analysis followed by Bonferroni post-test.

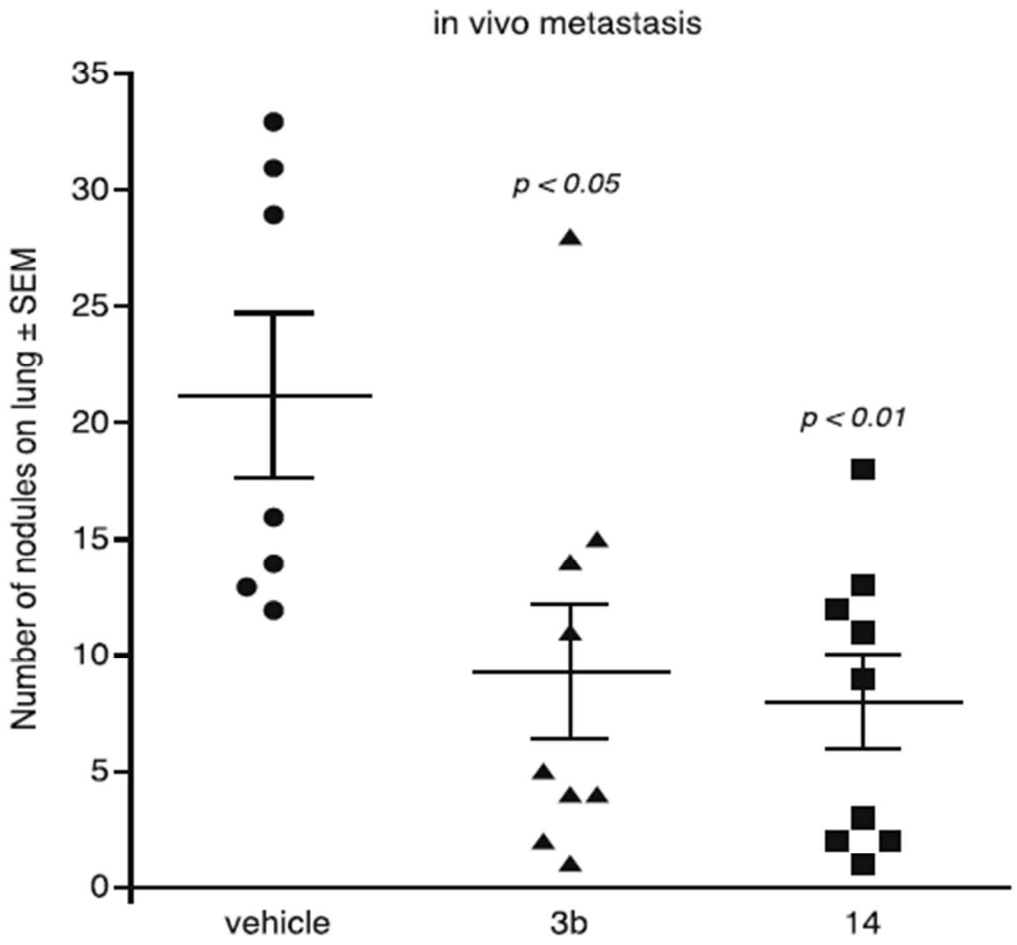

Figure 6 Effect of the various ATX inhibitors on the lung metastasis of B16F10 melanoma cells in C57BL/6 mice. Mice were treated daily with 1mg/kg of compound for up to 10 days. All mice were sacrificed at day 21 and the number of metastatic lung nodules was counted. Differences between groups were determined by 1-way ANOVA followed by Bonferroni post-test.

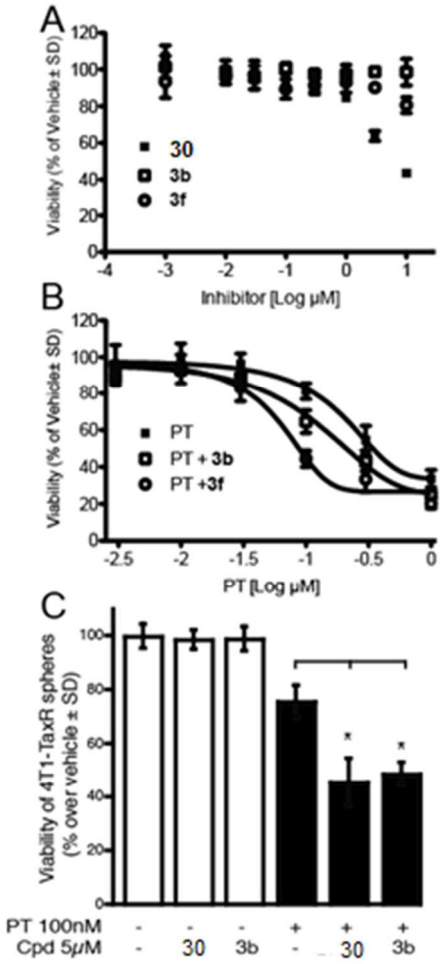

Figure 7. Effect of ATX inhibitors on the therapeutic resistance of 4T1 breast carcinoma cells and cancer stem-like cells. Panel A. The rate of growth of 4T1 breast carcinoma cells grown in adherent cultures is unaffected by ATX inhibitors **30**, compound **3b**, and **3f**. Panel B. ATX inhibitors (3 µM) when added together with PT shift the dose response curve of cell killing to the left indicating that these inhibitors make 4T1 cells more sensitive to PT-induced death. Panel C. Mammospheres were generated from the 4T1-TaxR cell line and treated with PT at 100 nM with or without the presence of **30** and compound 3b at 5µM, respectively. All measurements were done in quadruplicates and data represent the mean ± SD of an experiment performed three times. * $p < 0.05$ relative to PT alone based on 1-way ANOVA followed by Bonferroni post-test).

Schemes

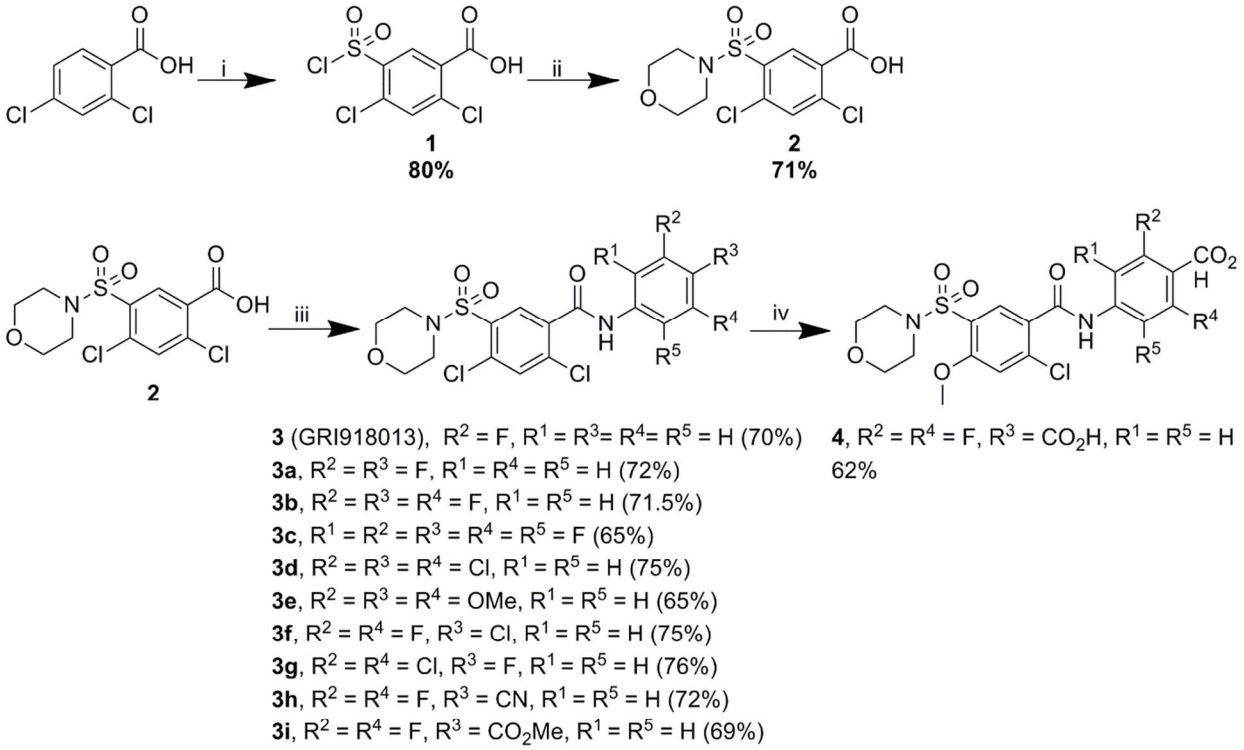

i. $ClSO_3H$, 12 hrs. reflux, ii. morpholine, Et_3N, R.T. 12 hrs. iii. a) $SOCl_2$, DMF (cat), 12 hrs. R.T. (b) substituted-aniline, pyridine, 12 hrs. R.T. iv) LiOH, MeOH/THF

Scheme 1. Design and synthesis of ring-A modified benzene sulfonamide analogues.

Percent yields are shown in parenthesis.

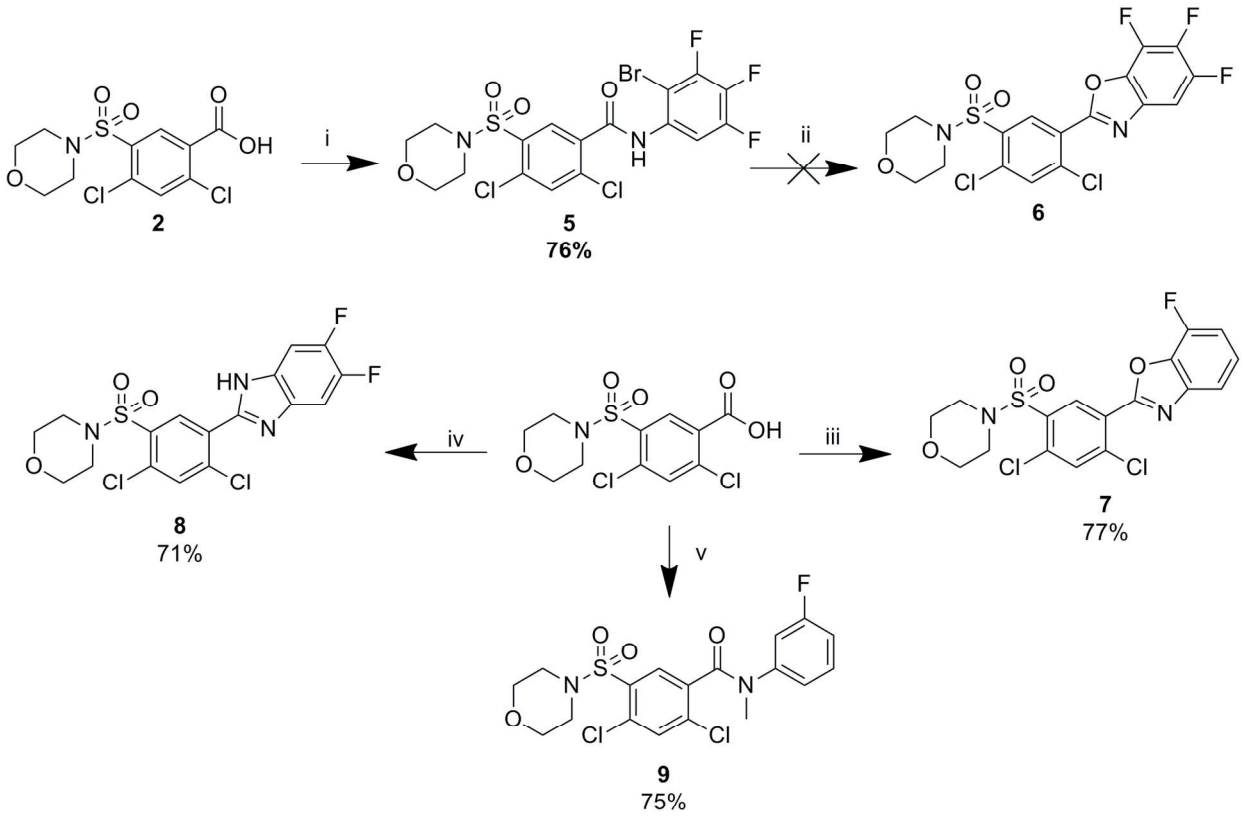

i. a) $SOCl_2$, DMF (cat), b) substituted-aniline, pyridine. ii) CuI (cat), 1,10-phenanthroline (cat), Cs_2CO_3, 2h hrs. reflux. iii. a) $SOCl_2$, DMF (cat), 12 hrs. R.T. b) substituted-aniline, Et_3N. c) p-TSA. H_2O, toluene, reflux. iv. $SOCl_2$, DMF (cat), 12 hrs. R.T. b) substituted-aniline, Et_3N. c) $POCl_3$, 100 min. reflux. v. $SOCl_2$, DMF (cat), b) N-methyl-substituted-aniline, pyridine

Scheme 2. Design and synthesis of amide bond modified benzene sulfonamide analogues.

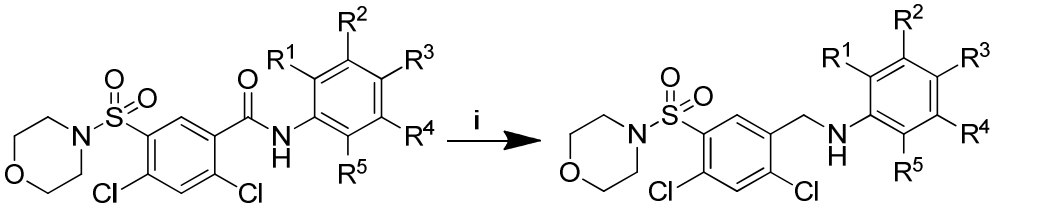

3a, $R^2 = R^3 = F$, $R^1 = R^4 = R^5 = H$
3b, $R^2 = R^3 = R^4 = F$, $R^1 = R^5 = H$

10, $R^2 = R^3 = F$, $R^1 = R^4 = R^5 = H$ (75%)
11, $R^2 = R^3 = R^4 = F$, $R^1 = R^5 = H$ (72%)

i. BH_3-DMS, THF (Sol), reflux 24hrs. to 72 hrs.

Scheme 3. Design and synthesis of reduced amide benzene sulfonamide analogues.

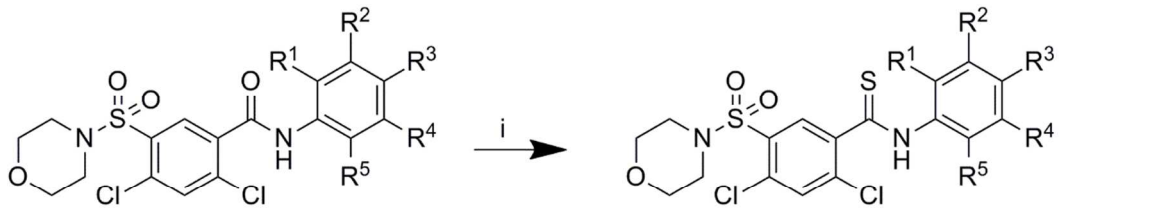

3, R^2 = F, R^1 = R^3= R^4= R^5 = H
3a, R^2 = R^3 = F, R^1 = R^4 = R^5 = H
3b, R^2 = R^3 = R^4 = F, R^1 = R^5 = H
3g, R^2 = R^4 = Cl, R^3 = F, R^1 = R^5 = H

12, R^2 = F, R^1 = R^3= R^4= R^5 = H (68%)
13, R^2 = R^3 = F, R^1 = R^4 = R^5 = H (70%)
14, R^2 = R^3 = R^4 = F, R^1 = R^5 = H (71%)
15, R^2 = R^4 = Cl, R^3 = F, R^1 = R^5 = H (72%)

i. Lawesson's reagent, toluene (sol), Reflux

Scheme 4. Design and synthesis of thioamide benzene sulfonamide analogues.

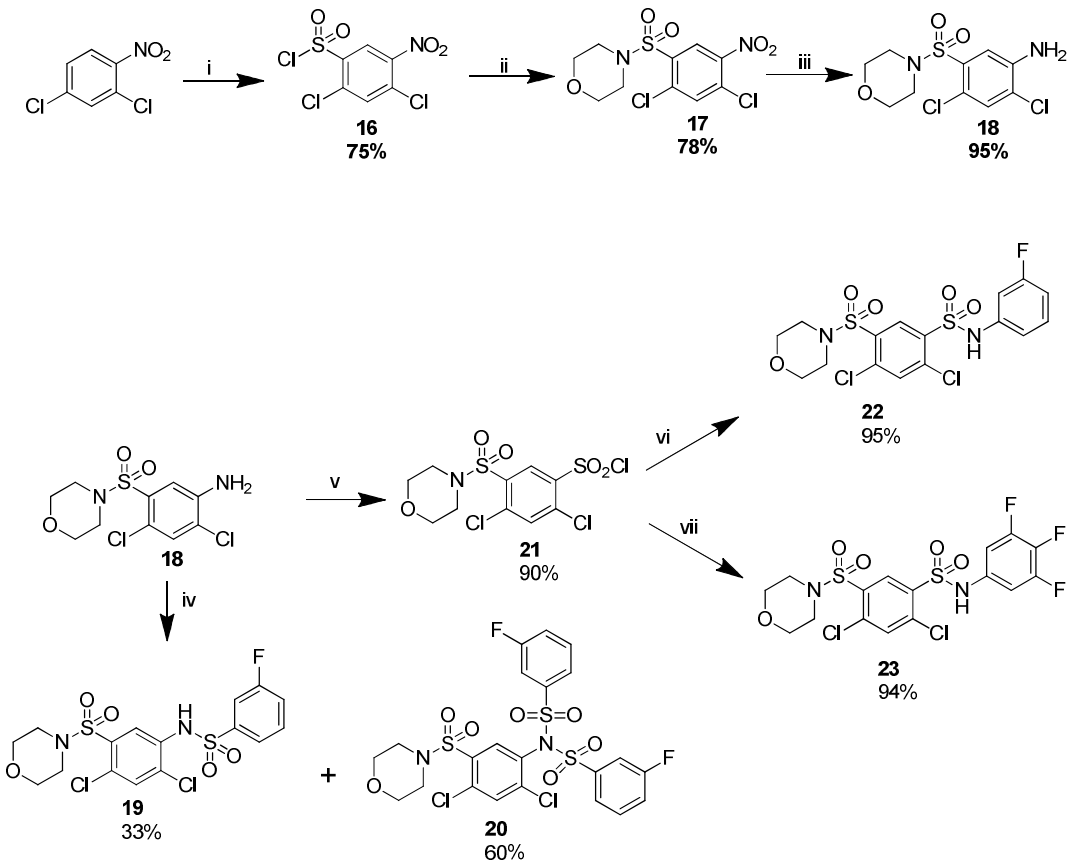

i. $ClSO_3H$, reflux, 12 hrs. ii. morpholine, Et_3N, R.T. 12 hrs. iii. iron powder, HCl, reflux, 5 hrs. iv. substituted-benzenesulfonyl chloride, Et_3N, DMAP, 96 hrs. v. $NaNO_2$, HCl, 0 ^{O}C, SO_2, CH_3CO_2H. vi. 3-fluoroaniline, Et_3N. vii. 3,4,5-trifluoro aniline, Et_3N.

Scheme 5. Design and synthesis of di-sulfonamide analogues.

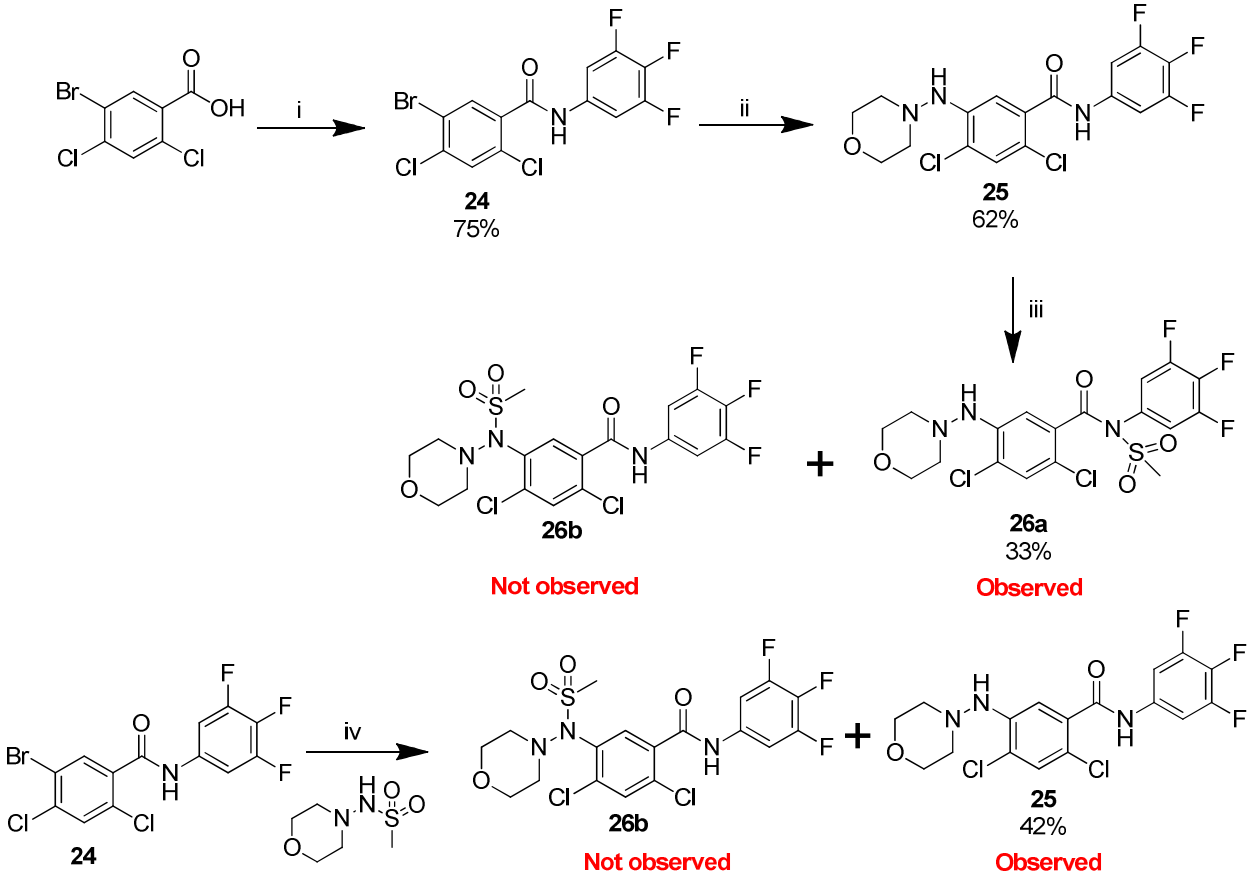

i. a) $SOCl_2$, DMF(cat), 12 hrs. R.T. b) 3,4,5-trifluoro-aniline, pyridine, 12 hrs. R.T. ii. 4-aminomorpholine, LiCl, $Pd_2(dba)_3$, Xantphos, NaOBu-t, 12 hrs. reflux. iii. NaOBu-t, methanesulfonylchloride, 24 hrs. R.T. iv. N-morpholinomethanesulfonamide, $[Pd(allyl)Cl]_2$, t-BuXphos, K_2CO_3

Scheme 6. Design and synthesis of hydrazine analogues.

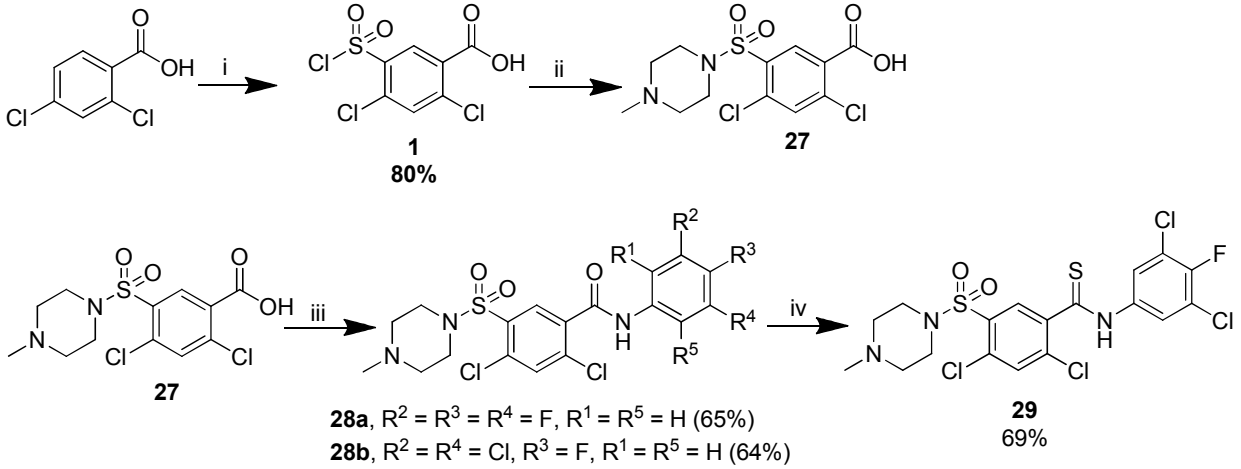

i. $ClSO_3H$, 12 hrs. reflux, ii. N-methylpiperazine, Et_3N, R.T. 12 hrs. iii. a) $SOCl_2$, DMF (cat), 12 hrs. R.T. (b) substituted-aniline, pyridine, 12 hrs. R.T. iv) Lawesson's reagent

Scheme 7. Design and synthesis of piperazine analogues.

TABLE OF CONTENTS GRAPHIC

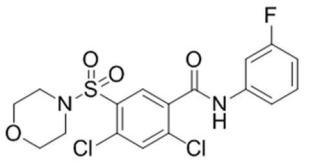

3, IC_{50} = 117 nM

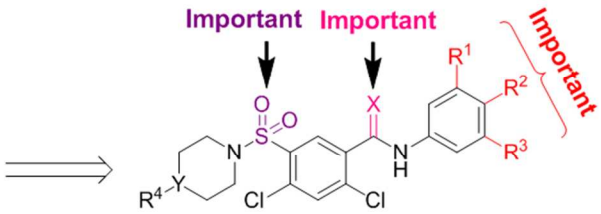

3b, IC_{50} = 9 nM, X = O, Y = O, R^1 = F, R^2 = F, R^3 = F
3a, IC_{50} = 32 nM, X = O, Y = O, R^1 = R^2 = F, R^3 = H
14, IC_{50} = 35 nM, X = S, Y = O, R^1 = F, R^2 = F, R^3 = F
3g, IC_{50} = 40 nM, X = O, Y = O, R^1 = Cl, R^2 = F, R^3 = C
3f, IC_{50} = 84 nM, X = O, Y = O, R^1 = F, R^2 = Cl, R^3 = F
28a, IC_{50} = 67 nM, X = O, Y = N, R^1 = Cl, R^2 = F, R^3 = Cl, R^4 = CH_3

~ 10 Examples with IC_{50} values less than 100 nM

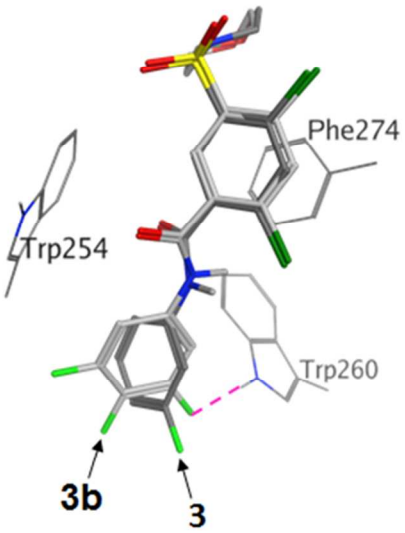

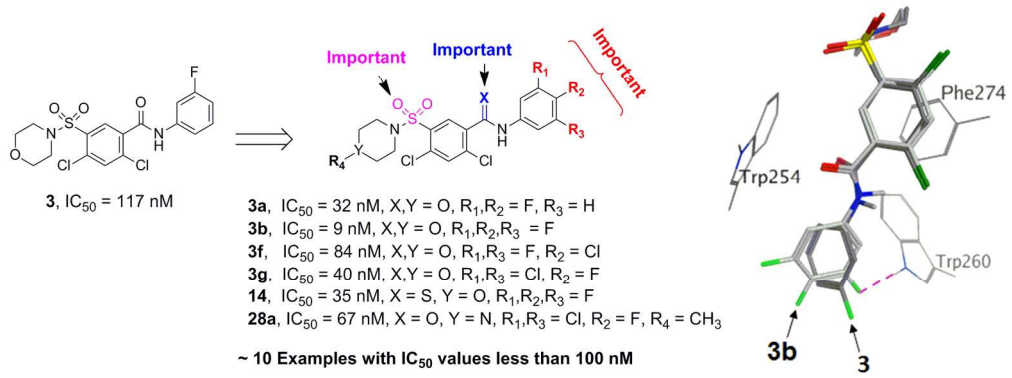

Table of Content Graphic

245x98mm (200 x 200 DPI)